NASA TN D-353

TECHNICAL NOTE
D-353

EXPERIMENTAL DETERMINATION OF THE RECOVERY FACTOR AND ANALYTICAL SOLUTION OF THE CONICAL FLOW FIELD FOR A 20° INCLUDED ANGLE CONE AT MACH NUMBERS OF 4.6 AND 6.0 AND STAGNATION TEMPERATURES TO 2600° R

By Frank A. Pfyl and Leroy L. Presley

Ames Research Center
Moffett Field, Calif.

NATIONAL AERONAUTICS AND SPACE ADMINISTRATION
WASHINGTON
June 1961

NATIONAL AERONAUTICS AND SPACE ADMINISTRATION

TECHNICAL NOTE D-353

EXPERIMENTAL DETERMINATION OF THE RECOVERY FACTOR AND ANALYTICAL SOLUTION OF THE CONICAL FLOW FIELD FOR A 20° INCLUDED ANGLE CONE AT MACH NUMBERS OF 4.6 AND 6.0 AND STAGNATION TEMPERATURES TO 2600° R

By Frank A. Pfyl and Leroy L. Presley

SUMMARY

The local recovery factor was determined experimentally along the surface of a thin-walled 20° included angle cone for Mach numbers near 6.0 at stagnation temperatures between 1200° R and 2600° R. In addition, a similar cone configuration was tested at Mach numbers near 4.5 at stagnation temperatures of approximately 612° R. The local Reynolds number based on flow properties at the edge of the boundary layer ranged between 0.1×10^4 and 3.5×10^4 for tests at temperatures above 1200° R and between 6×10^4 and 25×10^4 for tests at temperatures near 612° R.

The results indicated, generally, that the recovery factor can be predicted satisfactorily using the square root of the Prandtl number. No conclusion could be made as to the necessity of evaluating the Prandtl number at a reference temperature given by an empirical equation, as opposed to evaluating the Prandtl number at the wall temperature or static temperature of the gas at the cone surface.

For the tests at temperatures above 1200° R (indicated herein as the tests conducted in the slip-flow region), two definite trends in the recovery data were observed - one of increasing recovery factor with decreasing stagnation pressure, which was associated with slip-flow effects and one of decreasing recovery factor with increasing temperature. The true cause of the latter trend could not be ascertained, but it was shown that this trend was not appreciably altered by the sources of error of the magnitude considered herein.

The real-gas equations of state were used to determine accurately the local stream properties at the outer edge of the boundary layer of the cone. Included in the report, therefore, is a general solution for the conical flow of a real gas using the Beattie-Bridgeman equation of state. The largest effect of temperature was seen to be in the terms which were dependent upon the internal energy of the gas. The pressure and hence the pressure drag terms were unaffected.

INTRODUCTION

The transport of energy across the boundary layer surrounding bodies in flight has been the subject of intensive theoretical and experimental study. A significant number of the studies have been concerned with the amount of available energy absorbed by the body; hence the recovery-factor term has become considerably important. Although various theories have been developed for the prediction of the recovery factor, a lack of experimental data exists for high Mach numbers at the correct flight enthalpy levels.

The various theories as developed can be divided into two main groups. The first of these is applicable at low speeds (Mach numbers below 3.5). In these theories (see refs. 1, 2 and 3) air was considered to be a perfect gas with thermodynamic and transport properties invariant with temperature. This assumption led to the results of Crocco (ref. 1) who found that the recovery factor for a laminar boundary layer was predicted by the square root of the Prandtl number. A conclusion of this analysis was the invariance of the recovery factor with flight Mach number and Reynolds number.

A 3 1 8

The second approach was necessitated by the advent of flight speeds greater than Mach numbers of 3.5 wherein the assumption of constant thermodynamic and transport properties was no longer valid. Several authors (refs. 4 through 7), upon examining the basic energy transport processes, found, first, that the enthalpy rather than the temperature of the gas must by used in evaluating the recovery factor; secondly, the recovery factor for a laminar boundary layer could still be predicted by the square root of the Prandtl number, provided the Prandtl number is evaluated at a proper reference temperature. This approach then accounted for the real-gas effects (up to dissociation) and indicated that the recovery factor would be a function of both temperature and Mach number (see ref. 4).

The present investigation provides data showing the local recovery factor along a 20° cone at a free-stream Mach number near 6.0 and stagnation temperatures up to about 94 percent of flight stagnation temperatures. The data obtained are compared with the square root of the Prandtl number. The Reynolds number range of the tests conducted at high temperatures falls near the middle of the region defined by Tsien and others (see ref. 8) as the slip-flow region; consequently, the relations which can affect the recovery factor in slip flow are used. In the continuum region some data for a 20° cone at Mach numbers near 4.50 and temperatures of about 612° R are presented.

In the analysis of the high-temperature data, it was believed necessary to have accurate information concerning the conical flow field.

Consequently, a general solution for the conical flow using the Beattie-Bridgeman equation of state was developed to provide the needed information, and this solution is included herein (see appendix A).

NOTATION

A	area, ft^2
a	speed of sound, ft/sec
c_f	skin-friction coefficient
C_H	dimensionless heat-transfer coefficient
c_p	specific heat at constant pressure,[1] Btu/lb ^oR
c_v	specific heat at constant volume, Btu/lb ^oR
h	enthalpy,[2] Btu/lb
K	correction term (defined in eq. (B23) or in eq. (A10)
Kn	Knudsen number
k	thermal conductivity,[1] Btu/ft hr ^oR
k*	dependent variable given in equation (9)
l	length of cone, ft
M	Mach number
m	model wall thickness perpendicular to model axis, ft
Pr	Prandtl number, $\frac{\mu c_p}{k}$
p	pressure,[2] lb/ft^2
Q	heat transfer rate Btu/hr
Re	Reynolds number, $\frac{\rho U x}{\mu}$

[1]Without subscript m, the values for c_p, k, and ρ pertain to air.

[2]Without subscript t, the values for p, T, h, and ρ denote static conditions

R	gas constant, ft-lb/lb ^{o}R
r	recovery factor, $\frac{h_r-h_c}{h_{t_\infty}-h_c} = \frac{T_r-T_c}{T_{t_\infty}-T_c}$ (for c_p assumed constant)
T	absolute temperature,[2] ^{o}R
t	temperature, ^{o}F
U	velocity, ft/sec
X	mole fraction of particular species in a mixture of gases
x	distance along model longitudinal axis, ft
y	coordinate perpendicular to x axis, ft
γ	ratio of specific heats, $\frac{c_p}{c_v}$
ϵ	emissivity
θ	radius vector angle from axis of symmetry, deg
θ_v	characteristic temperature of vibrations, ^{o}R
μ	viscosity, lb/ft-hr
ξ	dependent variable given in equation (9)
ρ	density,[1,2] lb/ft^3
τ	time, hr
φ	cone half angle, deg

Subscripts

c	conditions at outer edge of the boundary layer along the cone surface
m	model material
n	normal to radius vector
s	shock wave

[1,2]See footnotes 1 and 2 p. 3.

t	total conditions (i.e., conditions that would exist if the gas were brought to rest isentropically)
tr	transverse curvature
w	conditions at the wall or surface of the model
∞	free-stream conditions
θ	a particular radius vector
$( )_{ZF}$	conditions employing zero flow and nearly zero pressure

Superscripts

–	slip flow; ideal gas flow in appendix A
'	quantities evaluated at the reference temperature T' (see eq. (6))

DESCRIPTION OF APPARATUS

Wind Tunnels

In this investigation two different wind tunnels were used to test two similar models. For the tests conducted at high temperatures, herein referred to as the hot-flow tests, a pebble-bed heater was employed in conjunction with the Ames Low-Density Wind Tunnel. Where the stream stagnation temperatures were just high enough to prevent liquefaction of the air components the tests were made in Ames 10- by 14-inch tunnel and are referred to as the cold-flow tests.

Hot-flow tests.- These tests were conducted in a Mach number 6.0, low-density, high-temperature wind tunnel (fig. 1) which had as a heat source zirconium-oxide pebbles (dia. = 3/8-inch) heated by natural gas burners. The pebbles were allowed to reach a maximum temperature of 4000° F. Surrounding the pebbles was an inner liner of insulating refractory which was contained in a steel shell fabricated in several sections. At the bottom and top of the shell, openings were provided for the entrance of the cold-storage air. A circular steel nozzle was placed in the center section of the steel shell. The nozzle, whose internal contours were obtained by the method of characteristics for a cold-flow Mach number of 6.0 (boundary-layer corrections applied), had an exit diameter of 4.296 inches and a throat diameter of 0.468 inch, and was 15.20 inches long. A water jacket surrounded the entire nozzle to keep the inner walls cool. The model was placed in an open-jet-type test section. Downstream of the test section a converging-type diffuser

was used to decelerate the flow. The air, upon leaving the diffuser, was cooled by a water injection system, and the desired back pressure was regulated by a five-stage steam-ejector system.

Cold-flow tests.- The Ames 10- by 14-Inch Supersonic Wind Tunnel was used for these tests. A complete description of the tunnel is given in reference 9.

Models and Instrumentation

Hot-flow tests.- The model used in these tests was a 20° included angle cone fabricated from type 416 stainless steel. A sketch of the model is shown in figure 2(a). The configuration was mounted on a transite end-plug locked to a hollow stainless-steel sting. (The transite material was used for the end-plug to insure negligible heat conduction losses out the base of the model.) Care was taken to prevent nonuniform circumferential heat conduction by maintaining a uniform wall thickness (the wall thickness was 0.025 in.). In order that a reliable value of emissivity could be used over the temperature range encountered, the external and internal surfaces of the model were plated with a thin coating of pure nickel and then "flashed" with platinum (ends of thermocouple were covered by the plating). A 3 1 8

Chromel-alumel thermocouples were embedded along the surface of the model and in the radiation shields which are shown in figure 2(a). Chromel-alumel was used because of its proven performance for measuring temperatures over a range from -300° to 2500° F. The thermocouple leads (wire size was No. 28 B and S gage) were brought out the sting and connected to indicating microvolt potentiometers. To insure consistent readings throughout the investigation, the model thermocouples were calibrated before and after each test against known controlled temperatures. During the tests the temperature-time history of the cone surface temperatures was obtained by photographing the indicating dials on the potentiometers. A 70-mm motion-picture camera capable of 20 frames per second was used with an electric timer placed in view of the camera.

A traversing mechanism inside the test chamber provided means for mounting several models and/or probes and moving these individually into the center of the air stream. The model for these tests was always placed at zero angle of attack with respect to the geometric center line of the nozzle.

The total temperature of the hot-flow air stream was measured by an aspirated double-shielded chromel-alumel thermocouple probe shown in figure 3. The thermocouple leads from the probe were connected to a standard potentiometer which was initially balanced against a standard cell. Concerning the measurement of the stagnation temperature, it was realized that effects such as radiation, conduction, and boundary-layer

phenomena along the probe could cause significant errors in obtaining a true stagnation temperature reading. The probe was designed to prevent these effects from influencing the true stagnation readings (see ref. 10 for a discussion of these types of temperature effects), and the thermocouple was calibrated against known temperatures.

The free-stream static pressure in the test section (assumed constant across the test section) was measured at two stations. One station, a wall orifice, was located 1/2-inch upstream of the nozzle exit. At the other station, two probes (alined perpendicular to the nozzle center line) were located just aft of the nozzle exit and out of the nozzle flow. The pressures at the wall orifice and one exit probe were recorded on Pirani gages. The other exit pressure was measured with a McLeod gage (see ref. 11 for a description of these gages). The stagnation pressure of the entering flow was measured by a standard U type mercury manometer.

Cold-flow tests.- The model used in the 10- by 14-inch wind tunnel was also a 20° included angle cone fabricated from type 416 stainless steel (fig. 2(b)). The model was sting-mounted in the tunnel test section at 0° geometric angle of attack.

The several temperatures along the surface were also measured with chromel-alumel thermocouples embedded at the various stations along the model (see fig. 2(b)). The thermocouple leads were connected to indicating microvolt potentiometers and the system was calibrated in the same manner as was indicated in the previous description of hot-flow tests. Instrumentation for determining total temperature and Mach number has been discussed in reference 9.

TEST PROCEDURE

Hot-Flow Tests

The tunnel was operated between temperatures of 1200° and 2600° R at stagnation pressures of approximately 6.6 and 12.4 psia. For each test condition the flow was assumed stabilized when the static-pressure data recorded by the one McLeod and two Pirani gages were identical. The Mach number was determined from the ratio of static- to total-pressure data. (Corrections were applied for the effect of caloric imperfections on the ratio of static pressure to total pressure.) Also, the Mach number was checked during several high-temperature runs by a flow visualization method in which the angle of the oblique shock originating at the cone apex could be obtained within ±0.2°. For all runs the average Mach number was found to be 5.92 with a maximum deviation of ±0.12.

When the flow was established, the shielded thermocouple (total-temperature probe) was placed in the center of the air stream, and the total temperature was recorded. The probe was removed and the model was rotated into position. The temperature of the model was then measured continuously until it remained constant with time at all stations (three surface and two radiation shield temperatures). Upon reaching equilibrium (approximately 10-13 minutes) the model was removed from the hot stream and the total temperature probe again was placed in the hot stream. The temperature of the hot stream was taken as the average of the two temperature probe readings. The difference between these readings was never greater than 60° F (a function of temperature distribution in the heater), but for 80 percent of the runs the difference was less than 30° F.

To determine the cone external radiation losses to the surroundings, the model was allowed to cool under conditions of zero flow and nearly zero pressure. For these tests the model was brought up to equilibrium temperature. Then, the tunnel pressure was quickly reduced to a pressure of less than 10 microns of mercury and the flow was shut off. Data were recorded continuously up to the time at which the model was within 50° to 100° F of its environmental temperature (usually a time interval of approximately 20 minutes). It was observed during these tests that the internal radiation was approximately zero since the temperature of the outer radiation shield was approximately the same as the temperature of the cone (see appendix B for the derivation of the radiation heat loss).

Cold-Flow Tests

In the 10- by 14-inch wind tunnel the data were obtained at Mach numbers between 4.41 and 4.59 (in conjunction with a different investigation) and the total temperature of the air, heated electrically, was of the order of 612° R. The Mach number was calibrated and adjusted as indicated in reference 9. It was believed that these data would be representative of cold-flow data obtained at $M \cong 6.0$ in the continuum flow region since the difference in Mach number should have no significant effect on the recovery factor.

In these tests, after several minutes the model reached equilibrium (assumed zero external and internal radiation losses) and the potentiometers which indicated the surface temperatures were photographed.

REDUCTION OF DATA

Hot-Flow Tests

Gas properties.- In the analysis of the aerodynamic heat-transfer measurements made during the present investigation, it was necessary to

determine the local stream properties at the outer edge of the boundary layer of the cone. Because of the high temperatures encountered during the present tests, the gas can no longer be considered thermally and calorically perfect (ideal) and real-gas equations of state must be used; thus a general solution for the conical flow of a Beattie-Bridgeman gas was developed. This solution is included in appendix A, and for comparison purposes table II shows the ideal and real-gas properties (up to dissociation) at the outer edge of the boundary layer for several cone angles at various temperature levels.

Recovery factor.- As mentioned previously, the significant quantity defining the recovery factor for high-temperature flows is the enthalpy of the air rather than the temperature. Thus the recovery factor is given by

$$r = \frac{h_r - h_c}{h_{t_\infty} - h_c} \tag{1}$$

The enthalpy terms h_c and h_{t_∞} refer to characteristics outside the boundary layer and in the free stream, respectively, and were calculated from the flow solutions developed in appendix A and from the wind-tunnel flow properties. The quantity h_r is the recovery enthalpy and is defined as the enthalpy of the air at the surface under the conditions of no heat transfer to or from the surface. The latter condition did not exist during the present investigation. Furthermore, the skin temperature of the cone rather than the enthalpy of the surface air was measured. It was necessary, therefore, to develop an involved set of equations to reduce the skin-temperature data to the desired recovery enthalpy. The development and discussion of the equations is presented in appendix B.

Briefly, the equation for the recovery enthalpy developed in appendix B can be written

$$h_r = h_w + K \tag{2}$$

where K may be considered a correction term, and accounts for the following effects:

(1) Radiation heat transfer from external and internal surfaces of the cone

(2) Convective heat transfer to the cone

(3) Conductive heat transfer along the cone in the longitudinal direction

In the derivation of K, account was taken of the fact that the Reynolds number was sufficiently small for the flow to be in the slip-flow

station was the same for five different Mach numbers tested between 4.41 and 4.59, and observation shows the axial temperature gradient along the cone to be negligible. The trend in the recovery factor (figs. 6(b) and 7) was found to be similar to that established in other cold-flow tests (see ref. 2); that is, the recovery factor is essentially independent of Mach number and Reynolds number, and for laminar flow can be predicted by the square root of the Prandtl number. Both the low value of the local Reynolds number, $Re < 2.5 \times 10^5$, and the close agreement of the experimental data and the $\sqrt{Pr}$ rule for the recovery factor in laminar flow, indicate that the flow over the cone was definitely laminar.

Hot-Flow Tests

The results of the hot-flow tests are presented in figures 8 through 11. In figure 8, distributions of surface temperature along the model are shown for each test condition. The time history of the surface temperature is given in figure 9 for one representative test condition. The recovery factors calculated from the basic data of figures 8 and 9 are presented in figures 10 and 11 as functions of stagnation temperature and Reynolds number (based on T'), respectively.

The recovery factors shown in figures 10 and 11 are in fair agreement in magnitude with the square root of the Prandtl number. However, because of the spread of the data, no unique agreement with either $\sqrt{Pr'}$ or $\sqrt{Pr_c}$ can be established ($\sqrt{Pr_c} \approx 0.85$). The data presented in figure 10 also indicate two consistent trends, one of increasing recovery factor with decreasing pressure, and one of decreasing recovery factor with increasing temperature. These trends will be discussed in the following paragraphs.

Effect of pressure on recovery factor.- The trend of increasing recovery factor with decreasing pressure (stagnation temperature constant) seems to be in agreement with the present theories. The over-all effect of lowering the Reynolds number from the range associated with continuum flow, through the transition and slip-flow regimes and into the free-molecule-flow regime is to raise the recovery factor gradually from its continuum value ($r \approx 0.85$, assuming laminar flow) to its free-molecule-flow value ($r \geq 1.0$, see ref. 8). For the present investigation, a reduction of stagnation pressure at constant stagnation temperature lowered the Reynolds number. Since the Reynolds numbers are in the slip-flow range (see fig. 4), an increase in the recovery factor with decreasing pressure would be expected. Also, it was ascertained that the assumptions involved in the data reduction have little effect on this trend.

Effect of temperature on recovery factor.- The other trend apparent in figure 10 is that the recovery factor decreased with increasing temperature. This trend is contrary to what might be expected in the slip-flow regime, as discussed previously, since the Reynolds number decreased with increasing temperature (constant pressure). From the data of the present investigation, however, it is difficult to ascertain the true cause of this trend. The data may represent the actual effect of temperature on recovery factor at higher temperatures or an apparent effect resulting from uncertainties in the experimental measurements or the assumptions involved in reducing the data. To see the effect of the various factors that may contribute to this result it is necessary to review briefly the basic nature of the investigation and to consider the assumptions involved in the data reduction.

The determination of the recovery factor (given by eq. (1)) is dependent upon a knowledge of the wall enthalpy under conditions of continuum flow and no heat transfer. For investigations at elevated temperatures wherein the model surface becomes heated and thus radiates energy, it is necessary either to cancel the radiation or to formulate an energy balance equation to determine the adiabatic wall enthalpy h_r.

Since the latter approach was taken, the value of the actual convective heat transfer $d\bar{Q}_{c_{tr}}$ was determined (all the terms except $d\bar{Q}_{c_{tr}}$ in the energy balance equation (B21) could be evaluated from the experimental data). The classical continuum convective heat transfer, then, was obtained from

$$dQ_c = \frac{d\bar{Q}_{c_{tr}}}{\xi} \tag{8}$$

where ξ is a variable and accounts for various effects of the low-density high-temperature flow field. In particular, for this investigation, ξ included the effects of changes in boundary-layer thickness, velocity profile, Maxwell reflection coefficient and thermal accommodation coefficient.

Once the classical heat transfer is known, the recovery factor in terms of the actual heat transfer, is expressed as

$$r = \frac{\frac{d\bar{Q}_{c_{tr}}}{\xi k^*} + h_w - h_c}{h_{t_\infty} - h_c} \tag{9}$$

where $d\bar{Q}_{c_{tr}}/\xi k^*$ is equal to K (see eq. (2)) and is given by equation (B24). (The term k^* is a function of the geometry and the flow field properties, and is, in effect, related to the classical heat-transfer coefficient.)

Since the assumptions involved in evaluating the term ξ can affect the value of the recovery factor, it is worthwhile to see what effect reasonable variations in these assumptions have upon the recovery-factor data presented herein. The first assumption involved the boundary-layer thickness. The boundary-layer thickness was evaluated by an empirical equation, (B19). If this thickness were thinner by either 15 or 75 percent from the value used herein (a reduction in thickness could be produced by either slip-flow effects or the use of a different base for the Reynolds number), the recovery at the high temperatures would be decreased by approximately 1 and 5 percent, respectively.

Secondly, the velocity profile of the boundary layer was assumed to be quadratic. Changing the order of the profile from second to first or to third produced virtually no change in the recovery factor for the range of Knudsen numbers of the test.

The Maxwell reflection coefficient, σ, and the thermal accommodation coefficient, α, were taken as 0.90 for these analyses. A variation of -10 percent (from 0.90) for σ and α produces a 1- and 2-percent increase, respectively, in the recovery factor. Very little is known, however, of the correct value of these parameters for the surface conditions and wall temperature of the present investigation. A discussion of these factors is given in reference 8 where they are indicated to be a function of wall temperature. This is especially important for the thermal accommodation coefficient since, at the wall temperatures herein, the internal vibrational energy was excited and this may have caused a much greater variation in α than considered.

Also, the accuracy of the basic experimental data could affect the recovery factor presented herein. The accuracy of the thermocouples for the wall measurement was taken as ± 1 percent, the manufacturer quoted accuracy. A 1-percent variation in wall temperature produces a corresponding 1-percent variation in recovery factor. The stagnation temperature was taken as that indicated by the probe. If the probe itself had a recovery factor and radiation losses, this value would be low, or if the pebble bed radiated to the probe, this value would be high. A ± 1-percent variation in stagnation temperature produced a ∓ 1-percent variation in recovery factor.

In the preceding paragraphs the factors affecting the behavior of the recovery factor in the high-temperature low-density range have been discussed briefly. Although no explanation can be given for the cause of the trend noted herein, it is evident that no single source or combination of sources of error of the magnitudes mentioned was able to alter appreciably the trend of decreasing recovery factor with increasing temperature. However, it must be remembered that the correct values of some of the parameters are unknown, especially the thermal accommodation coefficient, and sufficiently low value could completely alter the present trend. Corroborating these results with others must be postponed until other high-temperature data become available.

CONCLUDING REMARKS

Wind-tunnel tests were conducted to determine whether the recovery factor can be predicted by the simple square root of the Prandtl number rule at stagnation temperatures approaching those encountered in flight. Data were obtained for a Mach number of 4.5 at a stagnation temperature of about 600° R, and for a Mach number of 6.0 at stagnation temperatures between 1200° and 2600° R. The Reynolds number for all tests was less than 2.5×10^5 and for the Mach number 6.0 tests in particular, the Reynolds number was always less than 10^4, thus introducing slip-flow effects.

From the data shown, the Prandtl number rule is believed to be valid for estimating the recovery factor in the range of temperatures considered. The Prandtl number used herein is based on a reference temperature T'; however, because of the nature of the experimental data, no conclusion can be drawn as to the necessity of using this temperature, as opposed to say the static temperature of the gas at the cone surface.

The recovery-factor data of the hot-flow tests also indicated two definite trends: one of increasing recovery factor with decreasing pressure, and one of decreasing recovery factor with increasing temperature. The first trend was seen to be in agreement with the present theories; that is, in slip flow an increase in the recovery factor with decreasing pressure (or Reynolds number) would be expected. The second trend, that of decreasing recovery factor with increasing stagnation temperature, was shown to be contrary to what might be expected in the slip-flow regime since the Reynolds number decreased with increasing temperature. The cause of this trend could not be explained, but, it was pointed out that no single source or combination of sources of error of the magnitudes considered was able to alter appreciably the trend of decreasing recovery factor with increasing temperature. Therefore, this trend should be viewed with reservation until other high-temperature data become available for corroboration.

Ames Research Center
National Aeronautics and Space Administration
Moffett Field, Calif., Mar. 20, 1961

APPENDIX A

A THEORETICAL SOLUTION OF INVISCID CONICAL FLOW OF REAL GASES AT TEMPERATURES BELOW DISSOCIATION

A necessary prerequisite to the determination of the transfer of energy from a flowing gas to a body in contact with that gas is a thorough knowledge of the properties of the flow field. For flows of air wherein the local static temperatures are low, the air can be considered ideal, and convenient solutions exist for most simple flows. However, for local static temperatures greater than about 700° R, air can no longer be considered an ideal gas and it is necessary to develop an exact solution for the conical flow of a real gas.

Because the solution presented herein is of interest to the general field of high-temperature gas dynamics, it is presented in a manner to make it entirely independent of the experimental portion of this paper.

The solution, as discussed in this part, has been programmed for an IBM 704 computing machine and is available upon request to Ames Research Center.

Determination of the properties of a conical flow field involves the simultaneous solution of the following equations:

$$\frac{d}{d\theta}(\rho v \sin\theta) + 2\rho u \sin\theta = 0 \qquad \text{(Continuity)} \qquad \text{(A1)}$$

$$v = \frac{du}{d\theta} \qquad \text{(Irrotationality)} \qquad \text{(A2)}$$

$$u\,du + v\,dv + \frac{dp}{\rho} = 0 \qquad \text{(Momentum)} \qquad \text{(A3)}$$

$$h + \frac{u^2+v^2}{2} = h_t \qquad \text{(Energy)} \qquad \text{(A4)}$$

$$h = h(p,\rho) \qquad \text{(State)} \qquad \text{(A5)}$$

A suitable combination of equations (A1), (A2) and (A3) yields the well-known Taylor-Macoll equation for conical flow (see ref. 18)

$$\frac{d^2u}{d\theta^2} = \frac{a_\theta^2\left(u_\theta + \cot\theta\,\frac{du}{d\theta}\right)}{\left(\frac{dy}{d\theta}\right)^2 - a_\theta} - u_\theta \qquad \text{(A6)}$$

which is basic to the solution presented herein. The use of the above set of equations assumes that the gas is inviscid, is everywhere in thermodynamic equilibrium, and is isentropic before and after the shock wave.

The equation of state for the gas used in this paper is the Beattie-Bridgeman equation with provision for variable specific heats. Choice of this model for the gas was based on the following:

(1) This equation of state is an accurate representation of gas characteristics up to temperatures where dissociation (diatomic and polyatomic molecules) and ionization (monatomic molecules) are encountered.

A
3
1
8

(2) This equation is accurate at densities where intermolecular forces should be considered.

(3) Constants required in the Beattie-Bridgeman equation of state are available for a large number of gases.

Table I presents the constants needed to make the Beattie-Bridgeman equations applicable for a number of the more common gases of current interest. For a more complete table of the Beattie-Bridgeman constants see reference 19. Data pertaining to the vibrational energy levels of other gases can be obtained in references 20 and 21.

The discussion of the solution is divided into three main areas:

(1) Determination of flow characteristics ahead of the shock wave.

(2) Determination of flow characteristics immediately behind the shock wave.

(3) Determination of the flow field between the shock wave and the body.

DISCUSSION

Conditions Ahead of Shock Wave

In general, the conditions ahead of a shock wave are defined by one of two sets of three variables. In free-flight investigations the variables usually specified are velocity, static temperature, and static pressure. In wind-tunnel investigations the variables usually specified are Mach number, stagnation temperature, and stagnation pressure. The first set is used in this paper as the direct input to the calculation of the flow through shock waves. Hence, where the second set is specified, a considerable amount of calculation is required to transform these

variables into those of the first set with the inclusion of real-gas effects. The required transformation equations are the subject of this section, and as presented herein are solved by an iterative process.

In solving for the temperature and pressure that satisfy the set of initial conditions, recourse is made to the usual conditions of adiabatic reversible flow. However, to account for the differences between an ideal gas and the Beattie-Bridgeman gas (see ref. 22), the enthalpy, the entropic equation of state, and speed of sound equations are modified as follows:

$$h = J\bar{h} = J\bar{c}_p T \tag{A7}$$

$$\frac{p}{p_t} = \frac{\bar{p}}{p_t}\frac{K}{K_t} = \left(\frac{T}{T_t}\right)^{\frac{\bar{\gamma}}{\bar{\gamma}-1}}\left(\frac{K}{K_t}\right) \tag{A8}$$

$$a = \sqrt{I}\,\bar{a} = \sqrt{I\bar{\gamma}RT} \tag{A9}$$

The correction factor for the enthalpy equation is given by:

$$J = 1 + \frac{\bar{\gamma}-1}{\gamma}\left[G + \rho\left(B_o - \frac{2A_o}{RT} - \frac{4c}{T^3}\right)\right.$$

$$\left. + \rho^2\left(\frac{3}{2}\frac{A_o f}{RT} - \frac{5}{2}\frac{B_o c}{T^3} - B_o b\right) + \rho^3\left(\frac{2B_o bc}{T^3}\right)\right]$$

where G is given below in general form and the necessary constants are presented in table I for the gases considered of interest herein.

$$G = \frac{1}{T}\left[\sum_i \frac{d_i X_i \theta_{v_i}}{\exp(\theta_{v_i}/T) - 1}\right] \qquad i = 1,2,3,4$$

The correction factor for the entropic equation of state is given by:

$$K = \frac{E}{F}\left(1 + e_1\rho + e_2\rho^2 + e_3\rho^3\right) \tag{A10}$$

where e, E, and F are given below (see table I for necessary constants)

A3188

$$e_1 = B_o - \frac{A_o}{RT} - \frac{c}{T^3}$$

$$e_2 = \frac{A_o f}{RT} - B_o b - \frac{B_o c}{T^3}$$

$$e_3 = \frac{B_o bc}{T^3}$$

A3188

$$E = \prod_i \left\{ \frac{\exp\left[\frac{\theta_{v_i}/T}{\exp(\theta_{v_i}/T)-1}\right]}{1 - \exp(-\theta_{v_i}/T)} \right\}^{d_i X_i} \qquad i = 1,2,3,4$$

$$F = \exp\left[\rho\left(B_o + \frac{2c}{T^3}\right) + \rho^2\left(\frac{B_o c}{T^3} - \frac{B_o b}{2}\right) + \rho^3\left(\frac{2}{3}\frac{B_o bc}{T^3}\right)\right]$$

The correction factor for the speed of sound is given by:

$$I = \frac{\gamma}{\bar{\gamma}}\left(1 + 2e_1\rho + 3e_2\rho^2 + 4e_3\rho^3\right) \qquad \text{(A11)}$$

In order to calculate the above correction factors, the density and specific heats of the gas must be calculated for the Beattie-Bridgeman gas. The density is given by

$$\rho = \frac{p}{RT}\left(1 + g_1 p + g_2 p^2 + g_3 p^3\right) \qquad \text{(A12)}$$

where

$$g_1 = -\frac{e_1}{RT}$$

$$g_2 = \frac{2e_1^2 - e_2}{(RT)^2}$$

$$g_3 = \frac{[5e_1(e_2 - e_1^2) - e_3]}{(RT)^3}$$

The specific heat at constant volume is given by:

$$c_v = \overline{c}_v + c_{vib} + \frac{6Rc}{T^3}\rho\left(1 + \frac{B_o}{2}\rho - \frac{B_o b}{3}\rho^2\right) \tag{A13}$$

where c_{vib} is given below and $\overline{c}_v$ as well as the constants for c_{vib} are given in table I.

$$c_{vib} = R\sum_i d_i X_i \left[\frac{\theta_{v_i}/2T}{\sin h(\theta_{v_i}/2T)}\right]^2$$

The specific heat at constant pressure is given by

$$c_p = c_v + R\left[\frac{\left(1 + \frac{2c}{T^3}\rho\right)\left(1 + B_o\rho + B_o b\rho^2\right)}{1 + 2e_1\rho + 3e_2\rho^2 + 4e_3\rho^3}\right] \tag{A14}$$

The ratio of specific heats, γ, is by definition

$$\gamma = \frac{c_p}{c_v} \tag{A15}$$

Since the forms are known for the various correction factors and thermodynamic properties for the Beattie-Bridgeman gas, the iterative process to determine the static temperature, static pressure, and velocity proceeds in the following manner. As a first approximation, the static temperature and pressure are taken as the ideal-gas values; namely,

$$\overline{T} = T_t\left(1 + \frac{\overline{\gamma}-1}{2}M^2\right)^{-1} \tag{A16}$$

$$\overline{p} = p_t\left(1 + \frac{\overline{\gamma}-1}{2}M^2\right)^{-\frac{\overline{\gamma}}{\overline{\gamma}-1}} \tag{A17}$$

The values for static temperature and pressure are then used to calculate the correction factors for the Beattie-Bridgeman gas. The static temperature for the Beattie-Bridgeman gas is then found from

$$T = \frac{T_t J_t}{J}(1-X) \tag{A18}$$

where

$$X = \frac{M^2}{M^2 + \frac{2}{\bar{\gamma}-1}\frac{J}{I}}$$

The static pressure is found from

$$p = p_t \left(\frac{T}{T_t}\right)^{\frac{\bar{\gamma}}{\bar{\gamma}-1}} \frac{K}{K_t} \tag{A19}$$

A
3
1
8

and the velocity is given by

$$U = Ma \tag{A20}$$

The degree of accuracy of the temperature and pressure given by equations (A18) and (A19) is dependent upon the initially assumed values given by equations (A16) and (A17). It is usually necessary to iterate the solution which involves using the values calculated in equations (A18) and (A19) to re-calculate the correction factors and then repeat the solution of equations (A18) and (A19).

The significant characteristics ahead of the oblique shock which are required to calculate the flow immediately behind the oblique shock are the vectoral quantities $T_{t_{\infty_n}}$, $P_{t_{\infty_n}}$ and M_{∞_n}. The use of the vectoral quantities perhaps bears some explanation. When the momentum and energy equations normal to the wave are written

$$P_\infty + \rho_\infty U_{\infty_n}{}^2 = \text{const} = P_{t_{\infty_n}} \tag{A21}$$

$$h_\infty + \frac{U_{\infty_n}{}^2}{2} = \text{const} = h_{t_{\infty_n}} = h(T_{t_{\infty_n}}, P_{t_{\infty_n}}) \tag{A22}$$

it is observed that the normal stagnation conditions must be used. These quantities in general are different from the free-stream Mach number and stagnation conditions. The normal Mach number is given by:

$$M_{\infty_n} = M_\infty \sin \theta_s \tag{A23}$$

The evaluation of the stagnation temperature and pressure normal to the shock wave proceeds as follows, where the static conditions and Mach number are given in equations (A18), (A19) and (A23), respectively.

The stagnation temperature normal to the shock wave is given by

$$T_{t_{\infty_n}} = \frac{T_\infty J_\infty}{J_{t_{\infty_n}}(1-X)} \tag{A24}$$

where X is evaluated for M_{∞_n}. The stagnation pressure normal to the shock wave is given by

$$p_{t_{\infty_n}} = \frac{pK_{t_{\infty_n}}}{K_\infty \left(\frac{T_\infty}{T_{t_{\infty_n}}}\right)^{\frac{\bar{\gamma}}{\bar{\gamma}-1}}} \tag{A25}$$

As a first approximation to the above temperatures and pressures, the ideal gas values of

$$T_{t_{\infty_n}} = T_\infty \left(1 + \frac{\bar{\gamma}-1}{2} M_{\infty_n}^2\right) \tag{A26}$$

and

$$p_{t_{\infty_n}} = p_\infty \left(1 + \frac{\bar{\gamma}-1}{2} M_{\infty_n}^2\right)^{\frac{\bar{\gamma}}{\bar{\gamma}-1}} \tag{A27}$$

can be used where T and P are the free-stream values determined previously ((A18), (A19)). This solution is also iterated until sufficient agreement is found.

Conditions Immediately Behind Shock Wave

If the conditions in front of the shock wave are known, the static temperature and pressure behind the shock wave can be found by an iterative solution. As a first approximation, the following values can be used:

$$\bar{T}_s = T_\infty \left\{ \frac{[2\bar{\gamma}M_{\infty_n}^2 - (\bar{\gamma}-1)][(\bar{\gamma}-1)M_{\infty_n}^2 + 2]}{(\bar{\gamma}+1)^2 M_{\infty_n}^2} \right\} \tag{A28}$$

and

$$\bar{p}_s = p_\infty \left[\frac{2\bar{\gamma}M_{\infty_n}^2 - (\bar{\gamma}-1)}{\bar{\gamma}+1} \right] \tag{A29}$$

The density behind the shock wave is given by the following:

$$\left(\frac{\rho_\infty}{\rho_S}\right)^2 \left[X_{\infty_n}\left(L_S - \frac{2\overline{\gamma}}{\overline{\gamma}-1}\right)\right] + \frac{\rho_\infty}{\rho_S}\left[X_{\infty_n}\left(\frac{2\overline{\gamma}}{\overline{\gamma}-1} - L_\infty\right) + L_\infty\right] - L_S = 0 \qquad (A30)$$

where

$$L = \frac{1}{J}\left(\frac{1}{1 + g_1 p + g_2 p^2 + g_3 p^3}\right)$$

A 3 1 8

The temperature and pressure for the Beattie-Bridgeman gas are then:

$$T_S = \frac{T t_{\infty_n} J t_{\infty_n}}{J_S}(1-X_S) \qquad (A31)$$

where

$$X_S = X_{\infty_n}\left(\frac{\rho_\infty}{\rho_S}\right)^2 \qquad (A32)$$

and

$$p_S = p_\infty\left[\frac{\rho_S L_S(1-X_S)}{\rho_\infty L_\infty(1-X_\infty)}\right] \qquad (A33)$$

Here again, the required agreement for successive values of T_S and p_S is obtained by iteration.

The total Mach number and velocity behind the shock wave are given by the following relation.

The normal Mach number behind the shock is:

$$M_{S_n} = M_{\infty_n}\sqrt{\frac{I_\infty}{I_S}\frac{T_\infty}{T_S}\left(\frac{\rho_\infty}{\rho_S}\right)^2} \qquad (A34)$$

The tangential Mach number is given by

$$M_{S,tan} = M_{\infty,tan}\sqrt{\frac{I_\infty T_\infty}{I_S T_S}} \qquad (A35)$$

and the total Mach number is then given by:

$$M_S = \sqrt{M_{S_n}^2 + M_S^2, \tan} \tag{A36}$$

The speed of sound behind the shock wave is given by:

$$a_S = \sqrt{\gamma R T_S} \tag{A37}$$

and the total velocity is

$$U = M_S a_S \tag{A38}$$

The stagnation conditions behind the shock wave are found from:

$$T_{t_S} = \frac{T_S J_S}{J_{t_S}(1-X_S)} \tag{A39}$$

where X is given by equation (A32), and from

$$p_{t_S} = \frac{p_S K_{t_S}}{K_S} \left(\frac{T_S}{T_{t_S}}\right)^{-\frac{\gamma}{\gamma-1}} \tag{A40}$$

The ideal-gas flow equations are used to determine the initial values of T_{t_S} and p_{t_S} used in the iterative solution of equations (A39) and (A40).

Conditions Between Shock Wave and Body

In the conical flow field, between shock wave and body, the velocity and hence temperature and pressure are constant along radial vectors from the cone apex. The solution of the conical flow field is then a step-by-step solution from one radius vector to the next.

The velocity along any radius vector is given by:

$$u_{\theta_i} = u_{\theta_{i-1}} + \left(\frac{du}{d\theta}\right)_{i-1} d\theta + \left(\frac{d^2u}{d\theta^2}\right)_{i-1} \frac{d\theta^2}{2} \tag{A41}$$

The velocity normal to the radius vector is given by:

$$v_{\theta_i} = \left(\frac{du}{d\theta}\right)_i = \left(\frac{du}{d\theta}\right)_{i-1} + \left(\frac{d^2u}{d\theta^2}\right)_{i-1} d\theta \tag{A42}$$

where the Taylor-Macoll equation is used as follows:

$$\left(\frac{d^2u}{d\theta^2}\right)_{i-1} = \left[\frac{a_\theta^2\left(u_\theta + \cot\theta\,\frac{du}{d\theta}\right)}{\left(\frac{du}{d\theta}\right)^2 - a_\theta^2} - u_\theta\right]_{i-1} \tag{A6}$$

A 3 1 8

The subscript i denotes any given radius vector, the first vector (at an angle $\theta_s - \Delta\theta$) being i=1 and so forth. The shock wave would then be i=0, at which the following boundary conditions are known:

$$\theta = \theta_s$$

$$u = U_\infty \cos\theta_s \tag{A43}$$

$$v = -M_{s_n} a_s$$

The entire solution is completed by numerical integration at each subsequent radial vector $(\theta - \Delta\theta)$ until the radius vector equals the cone surface half angle. The total velocity on any given radius vector is given by

$$U = \sqrt{u^2 + v^2} \tag{A44}$$

At this point in the solution, values for stagnation temperature (A39), stagnation pressure (A40), and velocity (A44) have been obtained. Hence, with the exception of Mach number, the same quantities are known as were used in determining the flow characteristics ahead of the shock wave. As a first approximation to the value of Mach number, the following is used:

$$M_\theta = \frac{U_\theta}{a_{\theta_{i-1}}} \tag{A45}$$

This value of Mach number and the stagnation temperature and pressure is then used in equations (A18) and (A19) to calculate the static temperature and pressure. Again this solution must be solved by iteration because of the approximation for Mach number.

A question that always arises is, what quantity, if any, can be used as a convenient and invariant normalizing parameter for the velocity. For this purpose, the only quantity that is truly invariant is the stagnation enthalpy, which is analogous to the square of the stagnation speed of sound of ideal-gas theory, and is a parameter used to normalize the velocity

$$W = \frac{U}{\sqrt{h_{t_\infty}}} \tag{A46}$$

The solution is continued until $v_\theta = 0$, which is the boundary condition for the cone surface.

In using a solution of this type, for any assumed values of M, and θ_s, the half-angle of the cone is unknown and given only by the complete solution. If the conditions for a cone of definite half-angle are desired, several solutions can be run, and the flow field for the cone interpolated between two solutions. Shown in table II are sample solutions for 10°, 20°, and 40° (half-angle) cones at 1000°, 2600°, and 3600° R.

The largest effect of increased temperature on the properties of a conical flow field is seen to be in the values affected by the internal energy of the gas (i.e., vibrational energy). The enthalpy is naturally expected to increase with temperature, and the calculations show, for the higher temperatures, significant changes in the specific heat, c_p, and γ. The pressure and, hence, the pressure drag are seen to be unaffected by temperature.

For the temperature and cone angle considered, the effects of increased temperature are seen to be small. However, for larger cone angles, or higher temperatures, considerable departure from the ideal-gas conical flow properties exist.

APPENDIX B

DEVELOPMENT OF EQUATION FOR RECOVERY FACTOR

As pointed out in the introduction, several authors have found that for flight speeds greater than a Mach number of 3.5 the enthalpy rather than the temperature of the gas must be used in evaluating the recovery factor. For such conditions then, the recovery factor is defined as

$$r = \frac{h_r - h_c}{h_{t_\infty} - h_c} \tag{B1}$$

The quantities h_c and h_{t_∞} were determined directly from the measurements of the flow characteristics of the wind tunnel, and the properties of the conical flow field were determined by the methods discussed in appendix A. The quantity h_r is the enthalpy of the air at the surface of the cone under the conditions of no heat transfer to or from the cone and of temperatures at equilibrium. The first condition did not exist during the present test. Furthermore, the skin temperature of the cone rather than the enthalpy term, h_r, was measured. Hence, it is necessary to use an involved set of equations to reduce the skin-temperature data to the desired enthalpy quantity, h_r. The development and discussion of these equations is the subject of this appendix.

To develop the equations for the recovery factor, it was necessary to determine the heat balance into and out of an incremental volume of the cone in the vicinity of the temperature-measuring station. The incremental volume, dV, shown in the sketch below is bounded by two sides having areas, A_1 and A_2, and the external and internal surfaces of area, A_e and A_i, respectively:

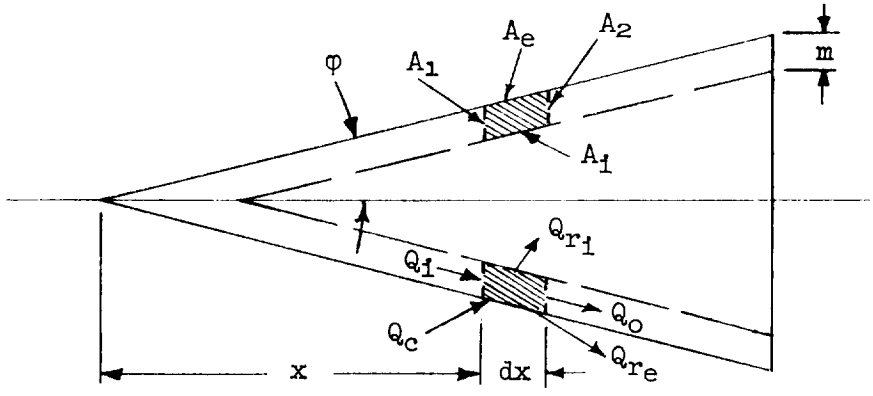

To the order of the differential length, dx, these areas and volumes can be expressed in terms of A_1, as follows

$$A_2 = A_1 + \frac{dA}{dx}\,dx \tag{B2}$$

$$dA_i = (A_1 - \pi m^2)\,\frac{dx}{m \cos \varphi} \tag{B3}$$

$$dA_e = (A_1 + \pi m^2)\,\frac{dx}{m \cos \varphi} \tag{B4}$$

$$dV = A_1 dx \tag{B5}$$

where

$$A_1 = \pi(2xm \tan \varphi - m^2)$$

and

$$\frac{dA}{dx} = 2\pi m \tan \varphi$$

The various heat flows comprising the net total heat to the volume, dV, are:

1. The conductive heat transfer along the metal skin, Q_i and Q_o.

2. The radiative heat transfer from the cone surfaces, Q_{r_i} and Q_{r_e}.

3. The convective heat transfer from the air to the cone surface, Q_c.

Each of these forms of heat transfer will be discussed in the following sections.

It should be noted that during the present tests, the cone temperatures used to determine the recovery factor were measured after the model reached equilibrium temperatures so that steady-state techniques were used in the following derivations.

CONDUCTIVE HEAT TRANSFER

In deriving the conductive heat-transfer equations, two assumptions were made:

1. No temperature gradient across the skin thickness.

2. No circumferential temperature gradient.

The equation for the conductive heat transfer into dV is given by:

$$Q_i = -k_m A_1 \frac{dT_w}{dx} \tag{B6}$$

and the heat transfer out is given by

$$Q_o = -k_m A_2 \frac{d}{dx}\left(T_w + \frac{dT_w}{dx}\,dx\right) \tag{B7}$$

A 3 1 8 (Note: The minus sign arises in equations (B6) and (B7) because x is in a direction of positive heat flow; that is, T_w decreases with positive x, so that dT_w/dx will always be negative. The minus sign must therefore be included for these equations to be compatible.)

The net transfer of heat by conduction to volume dV is then given by (neglecting second-order terms in dx)

$$dQ_{oi} = Q_i - Q_o$$

$$= k_m \left(\frac{dA}{dx}\frac{dT_w}{dx} + A_1 \frac{d^2T_w}{dx^2}\right) dx \tag{B8}$$

where A_2 has been expressed in terms of A_1; k_m is the thermal conductivity of the metal; and T_w is temperature measured at the wall.

The above equation requires a knowledge of the temperature gradient along the cone. In determining the values for dT_w/dx and d^2T_w/dx^2, the data for each thermocouple station were fitted to a second-order expansion of the form $T = ax^2 + bx + c$. In this way a consistent approach to obtaining the derivatives was assured.

Also required in the above equation is the thermal conductivity of the material. For the material used (stainless steel 416) the conductivity was obtained from reference 23. The variation with temperature of the conductivity is shown in figure 12.

RADIATION HEAT TRANSFER

Radiation to External Surroundings

For the present investigation, the radiation heat transfer was determined experimentally by allowing the model to cool in the wind tunnel under conditions of zero flow, a near vacuum, and tunnel-wall

temperatures the same as those used to measure the recovery factor. The temperature of the cone as it cooled was measured as a function of time and the quantity $(dT_w/d\tau)_{ZF}$ in relation to the cone temperature was obtained and is shown in figure 13. During these tests to determine the radiation heat transfer, it was noted that the temperatures at the three measuring stations along the cone surface and at the front radiation shield were the same, thus indicating no conductive heat transfer along the cone or internal radiation to the shield. Hence, the radiation heat transfer from dV to the external surroundings was given by:

$$dQ_{r_e} = -\rho_m c_{p_m} \left(\frac{dT_w}{d\tau}\right)_{ZF} dV$$

A 3 1 8

Substituting equation (B5) into the above equation gives

$$dQ_{r_e} = -\rho_m c_{p_m} A_1 \left(\frac{dT_w}{d\tau}\right)_{ZF} dx \tag{B9}$$

where

ρ_m density of material

c_{p_m} specific heat of material

τ time

Unfortunately, experimental data giving the specific heat of the material, c_{p_m}, as a function of temperature for stainless steel 416 could not be found in the literature. Consequently, the values used for c_{p_m} were derived from the empirical expression:

$$c_{p_m} = \sum w_i \frac{c_i}{M_i} \tag{B10}$$

where

w_i fraction of specie i

c_i molar heat capacity of specie i

M_i molecular weight of specie i

The chemical composition of the stainless steel is given in table III and values of c_{p_m} in relation to temperature are shown in figure 14. (As a matter of interest other values of k_m and c_{p_m} for different steels are presented in figures 12 and 14, respectively. Data are from references 24 to 28.) Note that the experimental c_p values for stainless 403 (composition nearly the same as 416, see table III) has a similar trend to that given by the theory for 416 and 403.

Radiation to Internal Shields

A 3 1 8

In contrast to those measurements made to determine the external radiation while the model was cooling, the temperature of the cone surface and the internal radiation shields were not the same for the steady state (flow-on) tests. The equation for thermal radiation between the internal surface of the cone and the radiation shield was derived using the approach of reference 2, and is given by

$$dQ_{r_i} = \epsilon\sigma(T_w^4 - T_s^4)(F_{i-s} + F_{s-i})dA_i$$

where

ϵ emissivity of unoxidized platinum

σ Stefan-Boltzmann constant

T_s temperature of front radiation shield, $^\circ R$

Evaluating the form factors gave:

$$F_{i-s} = \sin\varphi$$

$$F_{s-i} = 0$$

and if equation (B3) is substituted for dA_i, the internal radiation is given by:

$$dQ_{r_i} = \epsilon\sigma(T_w^4 - T_s^4)\sin\varphi\,\frac{(A_1 - \pi m^2)}{m\cos\varphi}\,dx \qquad \text{(B11)}$$

The emissivity, ϵ, is shown as a function of temperature in figure 15. The data were obtained from reference 29.

CONVECTIVE HEAT TRANSFER

In this section, the basic equation for convective heat transfer to a flat plate in continuum flow will be presented. Various correction terms to the basic equation will then be presented in order that the results be applicable to the present investigation.

Basic Equation

The equation for convective heat transfer to a flat plate incorporating the variation of the fluid properties with temperature is given by (see ref. 4)

$$dQ_c = 3600\, C_H \rho_c U_c (h_r - h_w)\, dA_e$$

where

C_H dimensionless heat-transfer coefficient

h_r recovery enthalpy

h_w enthalpy at wall

ρ_c air density at edge of boundary layer

U_c velocity at edge of boundary layer

and the factor 3600 converts the unit time from seconds to hours.

It will be noticed that the convective heat transfer is then proportional to the difference between the recovery enthalpy, which is required to determine the recovery factor, and the enthalpy at the wall, which can be computed from the temperature measurements made in the investigation.

Van Driest (ref. 4) calculated the dimensionless parameter, $C_H \sqrt{Re_c}$, for a laminar boundary layer on an insulated flat plate at various stagnation temperatures. His result is plotted in figure 16.

Expressing A_e in terms of A_1, the basic equation for the convective heat transfer becomes

$$dQ_c = 3600\, (C_H \sqrt{Re_c})\, \frac{\rho_c U_c}{\sqrt{Re_c}}\, (h_r - h_w)\, \frac{A_1 + \pi m^2}{m \cos \varphi}\, dx \qquad (B12)$$

Correction Factors Considered

The basic equation is for an insulated flat plate in continuum flow whereas in the present case, a cone in the slip-flow regime is being considered (see fig. 4). Correction factors are required to account for these differences. A summary of the theoretical and experimental approach of the effect of slip flow on heat transfer is given in reference 30 and the applicable equation is

$$\overline{Q}_c = Q_c \left(\frac{\overline{c}_f}{c_f}\right) B \tag{B13}$$

where the bar denotes slip flow and B is a function of the slip velocity ratio. In addition, the transverse curvature of the cone will have an effect on the skin friction. In reference 30 or 31 it was shown that when $\delta^* \cos \varphi / R$ is less than or of the order of unity (for the present tests $\delta^* \cos \varphi / R$, where δ^* is boundary-layer displacement thickness and R is local radius of external surface of cone, was always less than 0.30), the skin-friction coefficient, $c_{f_{tr}}$, is given by:

$$c_{f_{tr}} = G c_f$$

or

$$\overline{c}_{f_{tr}} = G \overline{c}_f \tag{B14}$$

where the subscript tr denotes transverse curvature.

Combining the correction factors and considering the effect of transverse curvature gives the convective heat transfer in the slip-flow region:

$$d\overline{Q}_{c_{tr}} = \sqrt{3}\, BG \left(\frac{\overline{c}_f}{c_f}\right) dQ_c \tag{B15}$$

where the factor $\sqrt{3}$ transforms the basic equation from that for a flat plate to that for a cone (see ref. 32).

The factor B is given by (see ref. 30):

$$B = \left[\frac{2 \frac{U_w}{U_c} \sqrt{Pr'} \left(1 - C_2 \frac{U_w}{U_c}\right) + \left(1 - \frac{U_w}{U_c}\right)^2 - \frac{\eta}{\sqrt{Pr'}} - C_1 \left(\frac{U_w}{U_c}\right)^2}{\left(1 - \frac{\eta}{\sqrt{Pr'}}\right)\left(1 - C_2 \frac{U_w}{U_c}\right)} \right] \tag{B16}$$

where

$$C_1 = \frac{8\gamma}{(\gamma + 1)\sqrt{Pr'}}\left(\frac{1 - \alpha}{\alpha}\right)\left(\frac{\sigma}{2 - \sigma}\right)$$

$$C_2 = 1 - \left(\frac{2\gamma}{\gamma + 1}\right)\left(\frac{\sigma}{2 - \sigma}\right)\left(\frac{2 - \alpha}{\alpha}\right)\frac{1}{Pr'}$$

$$\frac{U_w}{U_c} = \frac{n\left(\frac{2 - \sigma}{\sigma}\right)K_n}{1 + n\left(\frac{2 - \sigma}{\sigma}\right)K_n} \quad \text{(slip velocity ratio)}$$

A 3 1 8

$$\eta = \frac{T_w - T_c}{T_{t_\infty} - T_c}$$

and

n order of velocity profile

γ ratio of specific heats, $\frac{c_p}{c_v}$

σ Maxwell reflection coefficient

α thermal accommodation coefficient

Kn Knudsen number

Pr' Prandtl number evaluated at reference temperature

The factor G is given by (see ref. 31):

$$G = 1 + \xi\left[0.517 + 0.913\,\frac{T_w}{T_c} + 0.121(\gamma - 1)M_c^2\right]$$

where

$$\xi = \frac{1}{\sqrt{3}\tan\varphi}\sqrt{\frac{C_e}{Re_c}}$$

$$C_e = \frac{\mu_w}{\mu_c} \frac{T_c}{T_w}$$

and

μ coefficient of viscosity with subscripts w referring to wall and c to outer edge of boundary layer

The coefficient of viscosity, μ, is given by Sutherland's equation (ref. 12) as

A 3 1 8

$$\mu = 264.084 \times 10^{-5} \frac{T^{3/2}}{T + 202} \tag{B17}$$

The factor $(\bar{c}_f/c_f)$ is given by (see ref. 30)

$$\frac{\bar{c}_f}{c_f} = \frac{5.5[f(L)]^{1/2}}{(2 + L)} \tag{B18}$$

where

$$L = \frac{1}{Kn\left(\frac{2 - \sigma}{\sigma}\right)}$$

and

$$f(L) = \frac{L^2}{10} + \frac{8}{15}\left[\log_e\left(\frac{2 + L}{2}\right) - 1.0\right] + \frac{16 - L^3}{15(2 + L)}$$

The Knudsen number is required to evaluate several of the previous terms. The Knudsen number as used herein is defined as:

$$Kn = \frac{\lambda}{\delta}$$

where λ, the local mean free path, as determined from kinetic theory is given by

$$\lambda = 1.26\sqrt{\gamma}\,\frac{\mu}{\rho a}$$

and the boundary-layer thickness for an insulated flat plate (ref. 33) is given by

$$\delta = \frac{5.0\ x}{\sqrt{Re}} (1 + 0.08\ M^2) \tag{B19}$$

By the application of the Hantsche-Wendt (ref. 32) transformation from a flat plate to a cone the Knudsen number can be expressed as[1]

$$Kr = \frac{0.756\ M_c}{(1 + 0.08\ M_c^2)} \sqrt{\frac{\gamma_c}{Re'}} \tag{B20}$$

A 3 1 8

Correction Factors Neglected

The effect of boundary-layer displacement on heat transfer was neglected because it was found that for each test condition the hypersonic interaction parameter [$\bar{X} = M_\infty^3(\sqrt{C_e}/\sqrt{Re_c})$] never exceeded a value of 0.3 (see ref. 30). Such low values imply that the interaction between the boundary layer and inviscid flow region is weak.

ENERGY BALANCE

Since the data were taken at equilibrium conditions, the net heat transfer to the volume dV can be written as

$$0 = dQ_{oi} - dQ_{re} - dQ_{ri} + d\bar{Q}_{ctr} \tag{B21}$$

---

[1]The transformation gives for the cone values

$$\lambda_c = \sqrt{3}\ \lambda \text{ (see ref. 34)}$$

$$\delta_c = \delta/\sqrt{3} \text{ (see ref. 35)}$$

where λ and δ are the flat-plate values.

Substitution of equations (B8), (B9), (B11) and (B15) gives

$$0 = k_m \left(\frac{dA_1}{dx} \frac{dT_w}{dx} + A_1 \frac{d^2T_w}{dx^2} \right) dx + \rho_m c_{p_m} A_1 \left(\frac{dT_w}{d\tau} \right)_{ZF} dx$$

$$- \epsilon\sigma(T_w^4 - T_s^4) \sin \varphi \frac{(A_1 - \pi m^2)}{m \cos \varphi} dx$$

$$+ \sqrt{3}\, BG \left(\frac{\bar{c}_f}{c_f} \right) \left[3600 \left(C_H \sqrt{Re_c} \right) \frac{\rho_c U_c}{\sqrt{Re_c}} (h_r - h_w) \frac{(A_1 + \pi m^2)}{m \cos \varphi} dx \right] \tag{B22}$$

A 3 1 8

Thus, it is possible to write

$$h_r = h_w + K \tag{B23}$$

where K is the total correction to the measured enthalpy of the air at the wall to determine the recovery enthalpy.

In terms of the measured quantities,

$$h_w = \int_o^T c_p T_w$$

where c_p is the specific heat at constant pressure.

Solving equation (B22) for K gives

$$K = \left[6236\, BG \left(\frac{\bar{c}_f}{c_f} \right) \left(C_H \sqrt{Re_c} \right) \frac{\rho_c U_c (A_1 + \pi m^2)}{m \cos \varphi \sqrt{Re_c}} \right]^{-1} \left[-k_m \frac{dA_1}{dx} \frac{dT_w}{dx} \right.$$

$$\left. - k_m A_1 \frac{d^2T_w}{dx^2} - \rho_m c_{p_m} A_1 \left(\frac{dT_w}{d\tau} \right)_{ZF} + \epsilon\sigma(T_w^4 - T_s^4) \tan \varphi \left(\frac{A_1 - \pi m^2}{m} \right) \right] \tag{B24}$$

in which all terms can be calculated from the measured cone temperatures, wind-tunnel flow characteristics, and the relationships derived herein.

REFERENCES

1. Crocco, Luigi: The Laminar Boundary Layer in Gases. CF-1038, Translation by North American Aviation, Aerophysics Lab., 1948.

2. Jakob, Max: Heat Transfer. Vol. II. John Wiley and Sons, Inc., New York, 1957.

3. Kaye, Joseph: Survey of Friction Coefficients, Recovery Factors, and Heat-Transfer Coefficients for Supersonic Flow. Tech. Rep. 6418-5, Dept. of Mech. Engr., Mass. Inst. of Tech., Oct. 1, 1953.

4. Van Driest, E. R.: The Laminar Boundary Layer with Variable Fluid Properties. Rep. AL-1866, North American Aviation, Inc., 1954.

5. Crown, J. C.: The Laminar Boundary Layer at Hypersonic Speeds. NAVORD Rep. 2299, Apr. 1952.

6. Klunker, E. B., and McLean, F. E.: Effect of Thermal Properties on Laminar-Boundary-Layer Characteristics. NACA TN 2916, 1953.

7. Eckert, Ernst, R. G.: Survey on Heat Transfer at High Speeds. WADC Tech. Rep. 54-70, Apr. 1954.

8. Emmons, H. W.: Fundamentals of Gas Dynamics. Vol. III. High Speed Aerodynamics and Jet Propulsion. Princeton University Press, 1958.

9. Eggers, A. J., Jr., and Nothwang, G. D.: The Ames 10- by 14-Inch Supersonic Wind Tunnel. NACA TN 3095, 1954.

10. Temperature, Its Measurements and Control in Science and Industry-American Institute of Physics; Reinhold Publishing Corporation, 1941.

11. Dushman, Saul: Scientific Foundation of Vacuum Technique. John Wiley and Sons, Inc., New York, 1949.

12. Rubesin, M. W., and Johnson, H. A.: A Critical Review of Skin-Friction and Heat-Transfer Solutions of the Laminar Boundary Layer of a Flat Plate. Trans. ASME, vol. 71, no. 4, May 1949, pp. 383-388.

13. Anon.: Tables of Thermal Properties of Gases. National Bureau of Statistics, Circular 564, Nov. 1955.

14. Hansen, C. Frederick: Approximations for the Thermodynamic and Transport Properties of High-Temperature Air. NACA TN 4150, 1958.

15. Keyes, Frederick G.: The Heat Conductivity, Viscosity, Specific Heat and Prandtl Numbers for Thirteen Gases. Tech. Rep. 37, MIT, (Project Squid), 1952.

16. Tribus, Myron, and Boelter, L. M. K.: An Investigation of Aircraft Heaters. II - Properties of Gases. NACA WR W-9, 1942.

17. Keenan, Joseph H., and Kaye, Joseph: Gas Tables. John Wiley and Sons, New York, 1954.

18. Staff of the Computing Section (under the direction of Zdeněk Kopal): Tables of Supersonic Flow Around Cones. Tech. Rep. 1, Dept. of Elec. Engr., Mass. Inst. of Tech., 1947.

19. Hirschfelder, Joseph O., Curtiss, Charles F., and Bird, R. Byron: Molecular Theory of Gases and Liquids. John Wiley and Sons, Inc., New York, p. 254.

20. Herzberg, Gerhard: Spectra of Diatomic Molecules. D. Van Nostrand Co., Inc., New York, 1950.

21. Herzberg, Gerhard: Infrared and Raman Spectra. D. Van Nostrand Co., Inc., New York, 1959.

22. Randall, R. E.: Thermodynamic Properties of Gases: Equations Derived From the Beattie-Bridgeman Equation of State Assuming Variable Specific Heats. TR-57-10, Arnold Engr. Div., Aug. 1957.

23. Taylor Lyman, ed., Metals Handbook, 1954 Supplement. The American Society for Metals, Cleveland, Ohio.

24. Fieldhouse, I. B., Hedge, J. C., and Lang, J. I.: Measurements of Thermal Properties. WADC TR 58-274, Nov. 1958.

25. Douglas, Thomas B., and Dever, James L.: Enthalpy and Specific Heat of Four Corrosion-Resistant Alloys at High Temperatures. Jour. of Research of the National Bureau of Standards, vol. 54. no. 1, Jan. 1955, p. 18.

26. High Temperature Thermophysical Properties. Denver Research Institute, Tech. Rep. 1023, Mar. 10, 1959.

27. Fieldhouse, I. B., Hedge, J. C., Lang, J. I., and Waterman, T. E.: Thermal Properties of High Temperature Materials. WADC Tech. Rep. 57-487, Feb. 1958.

28. Smithells, C. J.: Metals Reference Book. Second ed., Interscience Publishers Inc., New York, 1955.

29. Handbook of Chemistry and Physics. Thirty-Sixth Edition, Chemical Rubber Publishing Co., p. 2693.

30. Nestler, D. E.: Survey of Theoretical and Experimental Determination of Skin Friction in Compressible Boundary Layers. Part V. The Effects of Slip Flow. R59SD343, Missile and Space Vehicle Department, General Electric Co., 1959.

31. Probstein, R. F., and Elliott, D.: The Transverse Curvature Effect in Compressible Axially-Symmetric Laminar Boundary-Layer Flow. Rep. 261, Dept. of Aero. Engr., Princeton University, Apr. 1954.

32. Bradfield, W. S.: Some Notes Regarding the Transformation of Boundary Layer Parameters in Axially Symmetric Supersonic Flow. EM-4, Aero. Engr. Dept., Univ. of Minn., July 9, 1951.

33. Howarth, L.: Concerning the Effect of Compressibility on Laminar Boundary Layers and Their Separation. Proc. Royal Soc., series A, vol. 194, no. 1036, July 28, 1948, pp. 16-42.

34. Drake, R. M., and Maslach, G. J.: Heat Transfer from Right Circular Cones to a Rarefied Gas in Supersonic Flow. Rep. HE-150-91, Inst. of Engr. Res., Univ. of Calif., 1952.

35. Davies, F. V., and Cooke, J. R.: Boundary-Layer Measurements on 10° and 20° Cones at M = 2.45 and Zero Heat Transfer. R.A.E. TN Aero. 2314, 1954.

TABLE I.- GAS CONSTANTS FOR BEATTIE-BRIDGEMAN EQUATIONS

Gas	Gas constant, R $\frac{\text{ft-lb}_f}{\text{lb}_m\ ^\circ\text{R}}$	$\bar{c}_v$, $\frac{\text{ft-lb}_f}{\text{lb}_m\ ^\circ\text{R}}$	A_o, $\frac{\text{ft}^6\text{-lb}_f}{\text{lb}_m^2\text{ft}^2}$	f, $\frac{\text{ft}^3}{\text{lb}_m}$	B_o, $\frac{\text{ft}^3}{\text{lb}_m}$	b, $\frac{\text{ft}^3}{\text{lb}_m}$	c, $\frac{\text{ft}^3\ ^\circ\text{R}^3}{\text{lb}_m} \times 10^{-4}$	θ_{v_1}, $^\circ$R	θ_{v_2}, $^\circ$R	θ_{v_3}, $^\circ$R	θ_{v_4}, $^\circ$R	d_1	d_2	d_3	d_4	X_1	X_2	X_3	X_4
Air	53.328	2.5R	841.63	0.01068	0.02549	-0.00609	13.9943	6071.76	4060.4	0	0	1	1	0	0	0.788	0.212	0	0
H_e	386.145	1.5R	732.54	.23956	.05605	0	.09339	0	0	0	0	0	0	0	0	0	0	0	0
H_2	766.394	2.5R	26143.56	-.0402	.16654	-.34635	2.33547	11073.98	0	0	0	1	0	0	0	1	0	0	0
N_2	55.132	2.5R	922.57	.01496	.02884	-.00395	14.0011	6071.76	0	0	0	1	0	0	0	1	0	0	0
O_2	48.268	2.5R	790.13	.01282	.02314	.00211	14.0078	4060.4	0	0	0	1	0	0	0	1	0	0	0
CO_2	35.104	2.5R	1403.22	.02595	.03812	.02633	140.0718	6082.49	1727.68	3469.35	0	1	2	1	0	1	1	1	0
NH_3	90.692	3R	4476.63	.16014	.03211	.17971	2615.06	8641.01	2506.22	8839.07	4213.7	1	1	2	2	1	1	1	1
CH_4	96.351	3R	4807.58	.01853	.05581	-.01585	74.7424	7545.05	3950.91	7819.76	3381.84	1	2	3	3	1	1	1	1

TABLE II.- REAL-GAS CONE SOLUTIONS FOR AIR

Parameter	Units	T_{t_∞}, $^\circ$R								
		1000	2600	3600	1000	2600	3600	1000	2600	3600
ϵ_c	deg	10	10	10	20	20	20	40	40	40
θ_s	deg	14.3596	14.3596	14.3565	24.0737	24.0625	24.0309	46.494	46.2143	46.00
P_{t_∞}	lb/ft^2	1,798.6	1,798.6	1,798.6	1,798.6	1,798.6	1,798.6	1,798.6	1,798.6	1,798.6
P_∞	lb/ft^2	1.140	1.078	.9868	1.140	1.078	.9868	1.140	1.078	.9868
T_∞	$^\circ$R	122.88	342.99	491.58	122.88	342.99	491.58	122.88	342.99	491.58
h_{t_∞}	ft-lb/lb_m	187,933.0	524,560.0	751,516.0	187,933.0	524,560.0	751,516.0	187,933.0	524,560.0	751,516.0
γ_∞	---	1.39972	1.39965	1.39900	1.39972	1.39965	1.39900	1.39972	1.39965	1.39900
M_c	---	4.9955	4.9951	5.0031	3.7639	3.783	3.8135	1.9312	2.0105	2.0681
W_c	---	2.0620	2.1899	2.2384	1.9425	2.0632	2.1091	1.4759	1.5739	1.6136
T_c/T_{t_∞}	---	.1683	.1807	.1868	.2629	.2816	.2891	.5773	.5979	.5984
T_c	$^\circ$R	168.32	469.76	672.56	262.85	732.09	1040.84	577.30	1554.66	2154.40
h_c	ft-lb/lb_m	31,398	87,643.0	125,411.0	48,691.0	136,518.0	195,866.0	107,743.0	298,904.0	426,310.0
p_c/P_∞	---	2.8085	2.8087	2.8090	7.4496	7.4463	7.4373	23.3047	23.2085	23.158
c_p	$\text{ft-lb/lb}_m\ ^\circ\text{R}$	186.67	186.83	188.06	186.664	186.748	194.489	187.280	206.678	217.66
γ_c	---	1.3997	1.3991	1.3952	1.3997	1.3936	1.3776	1.3978	1.3476	1.3243

TABLE III.- COMPOSITION OF STAINLESS STEEL 416 AND 403

Element	Composition, percent,	
	416	403
Carbon, C	0.15	0.15
Chromium, Cr	13.00	13.00
Iron, Fe	83.97	84.85
Manganese, Mn	1.00	1.00
Molybdenum, Mo	0.60	---
Nickel, Ni	---	0.50
Phosphorus, P	0.04	---
Silicon, Si	1.00	0.50
Sulfur, S	0.24	---

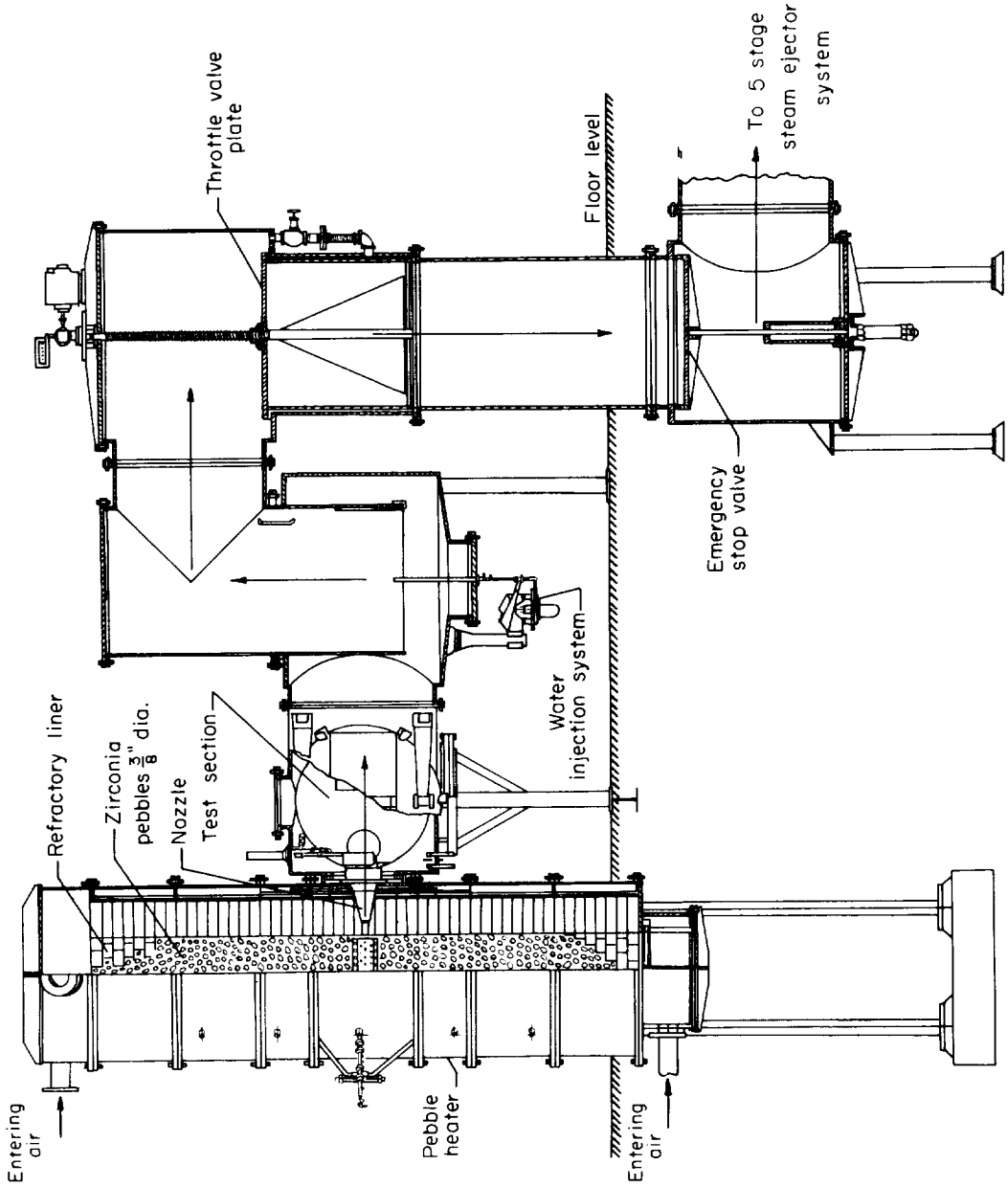

Figure 1.- Pebble-bed heater and low-density wind tunnel details.

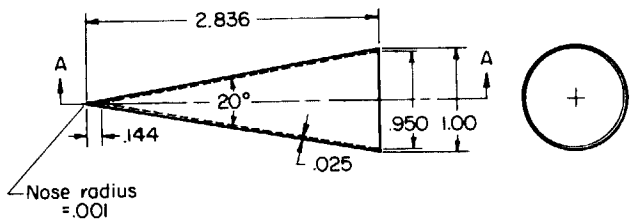

Cone details

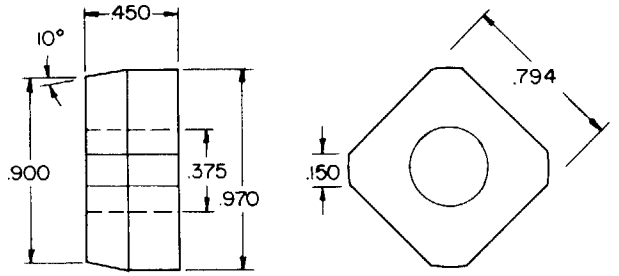

Transite end support plug

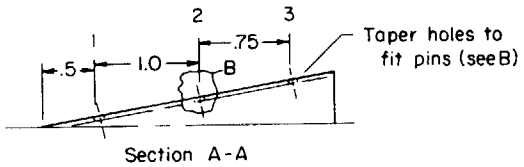

Thermocouple spacing & details

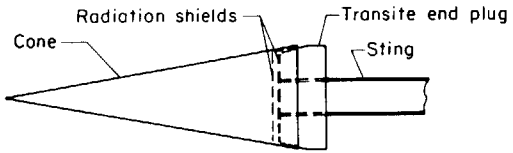

Hot-flow model

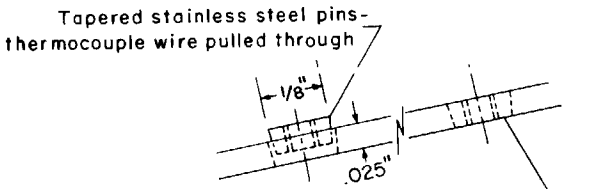

Detail B

Note: All dimensions in inches unless otherwise noted

Note: Both shields plated with nickel and flashed with platinium. Both shields fit into end of cone.

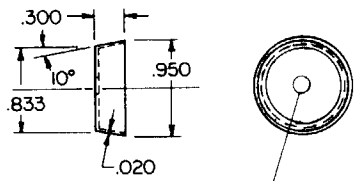

Radiation shields

(a) Hot-flow model.

Figure 2.- Model and instrumentation details.

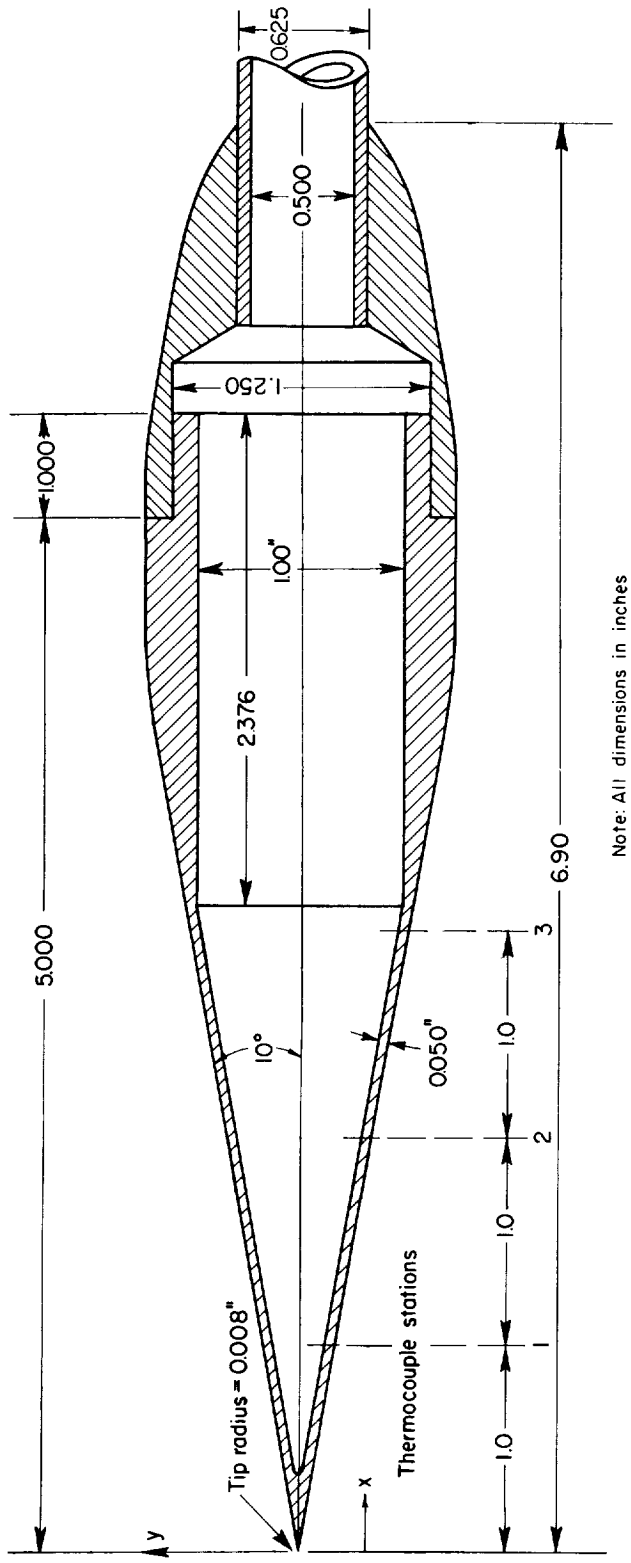

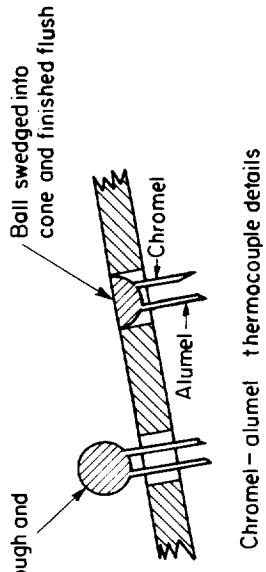

(b) Cold-flow model.

Figure 2.- Concluded.

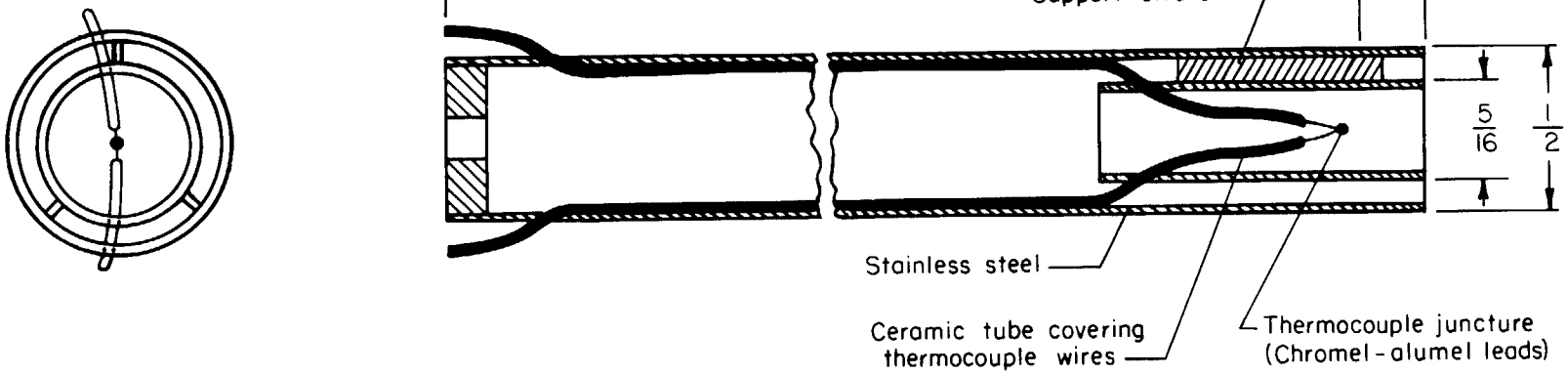

Total temperature measuring probe

Figure 3.- Details of temperature probe.

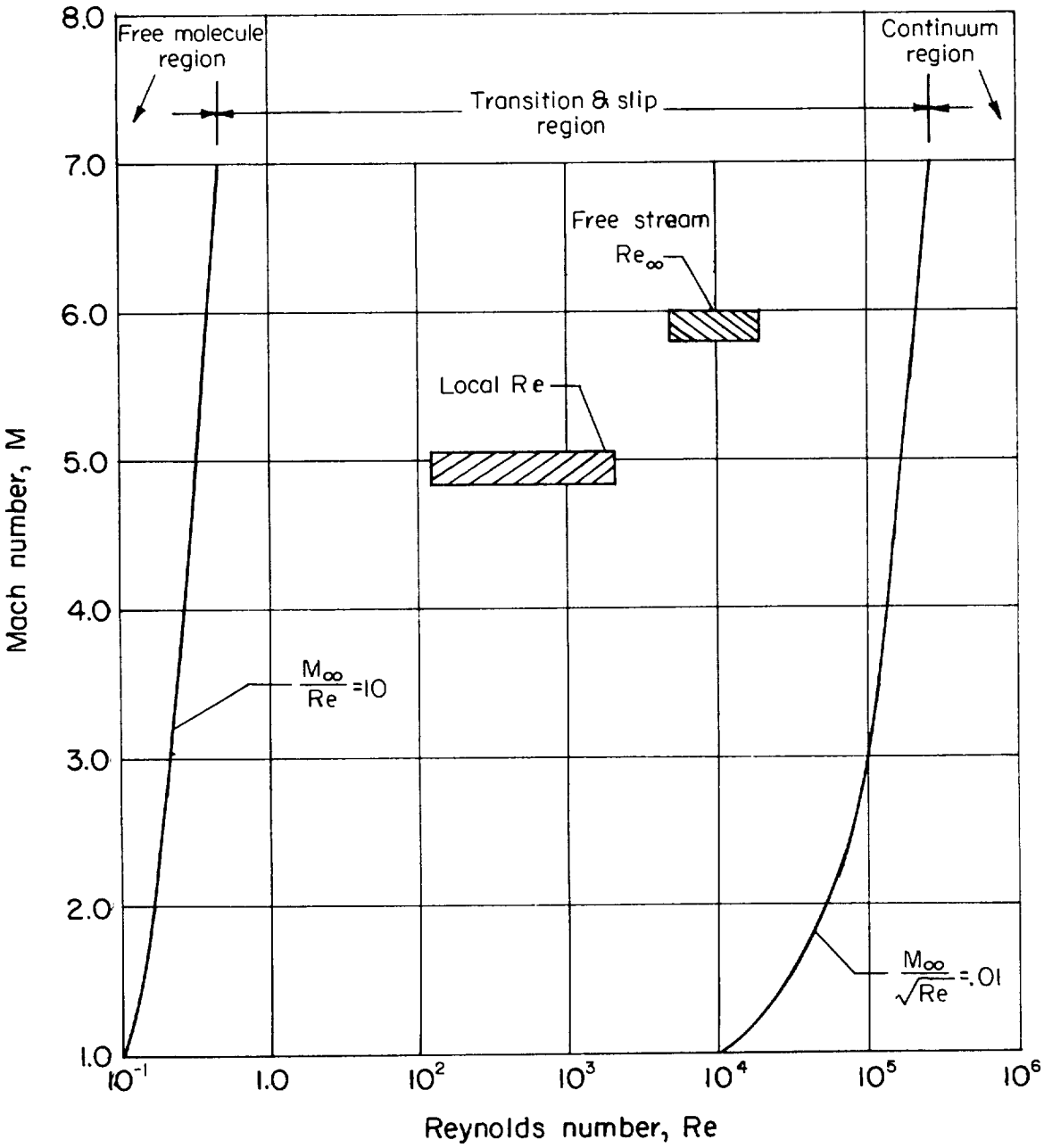

Figure 4.- Flow regions of investigation for hot-flow tests.

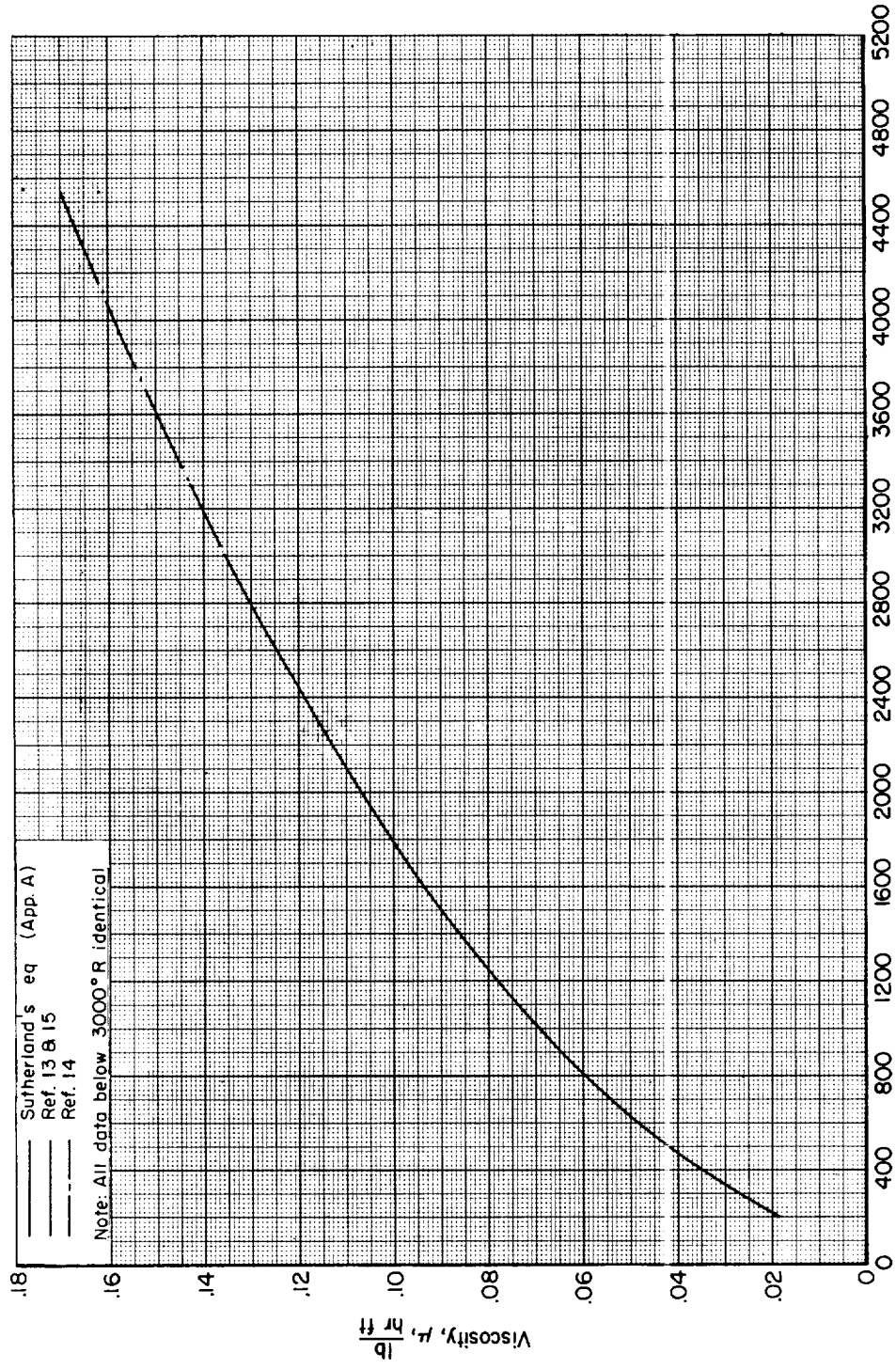

(a) Viscosity, μ.

Figure 5.- Transport and thermodynamic properties of air as a function of temperature.

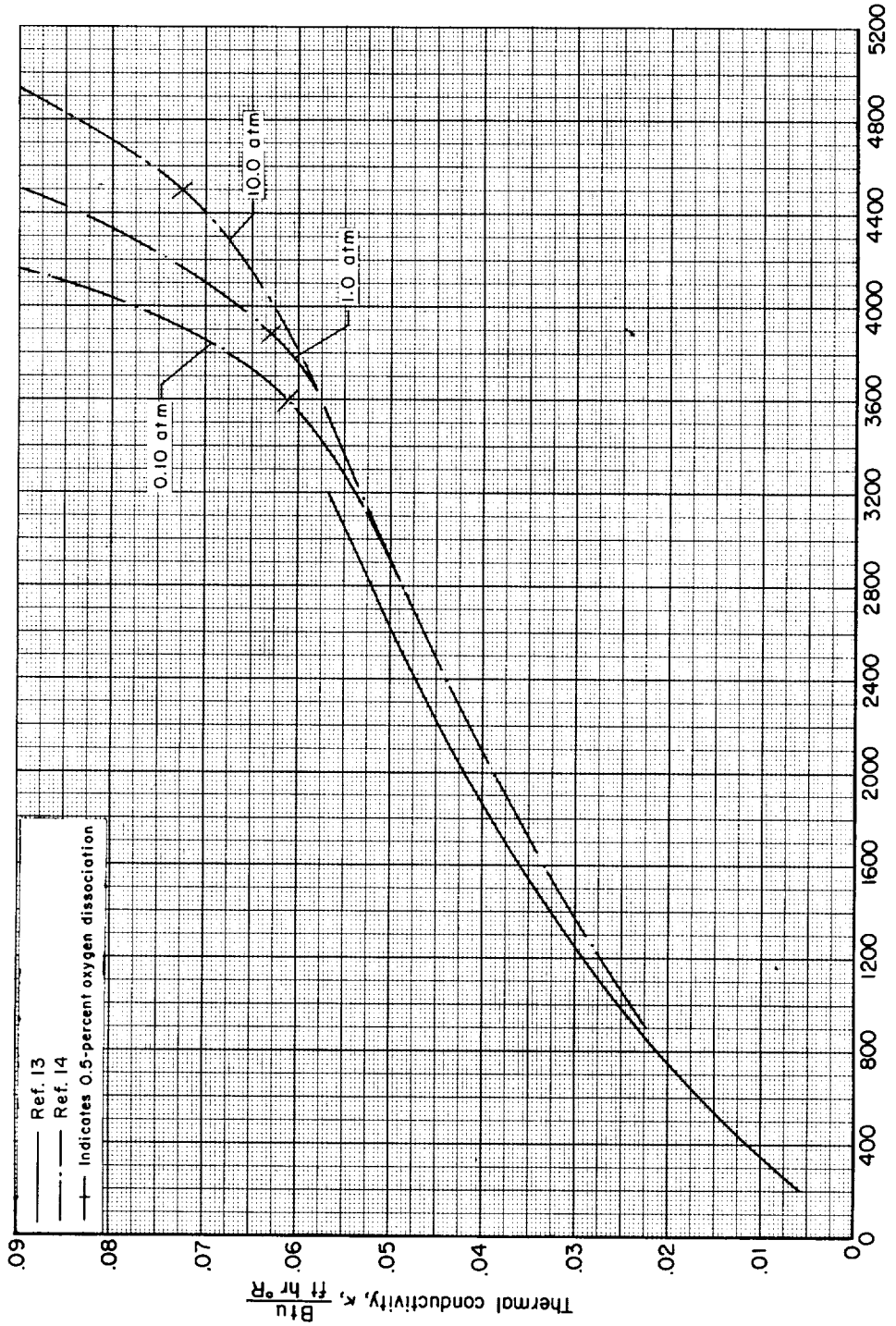

(b) Thermal conductivity, k.

Figure 5.- Continued.

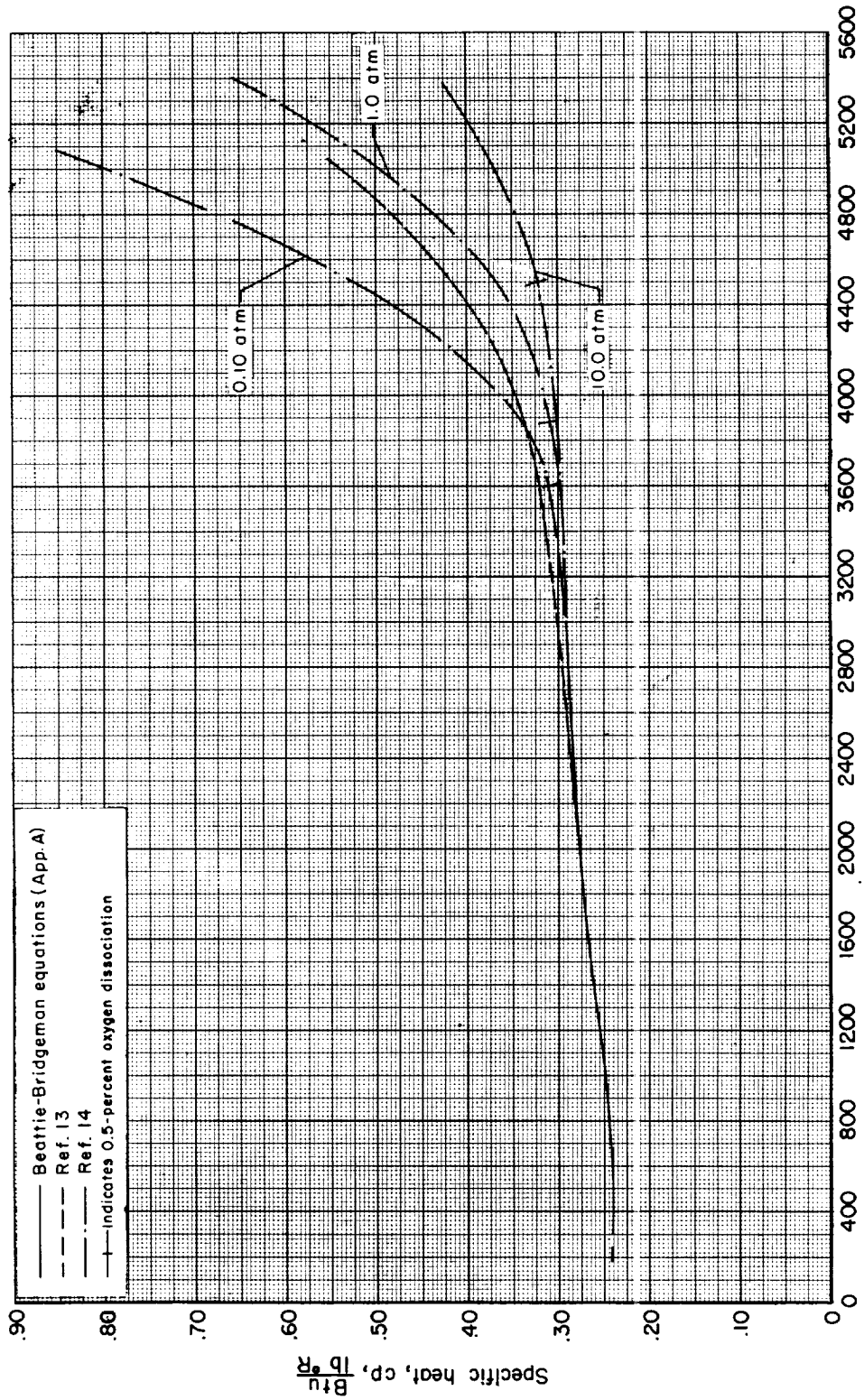

(c) Specific heat at constant pressure, C_p.

Figure 5.- Continued.

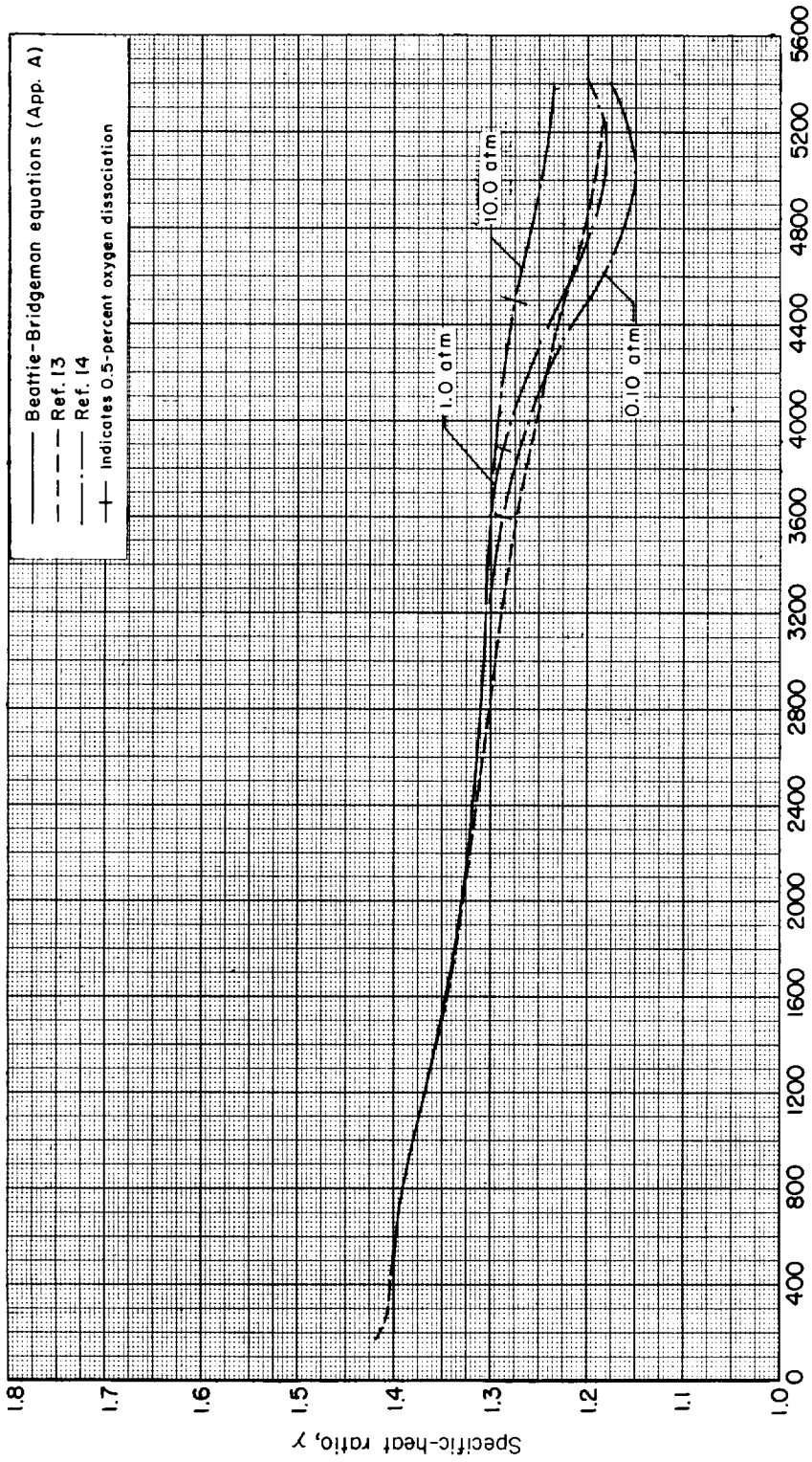

(d) Specific-heat ratio, γ.

Figure 5.- Continued.

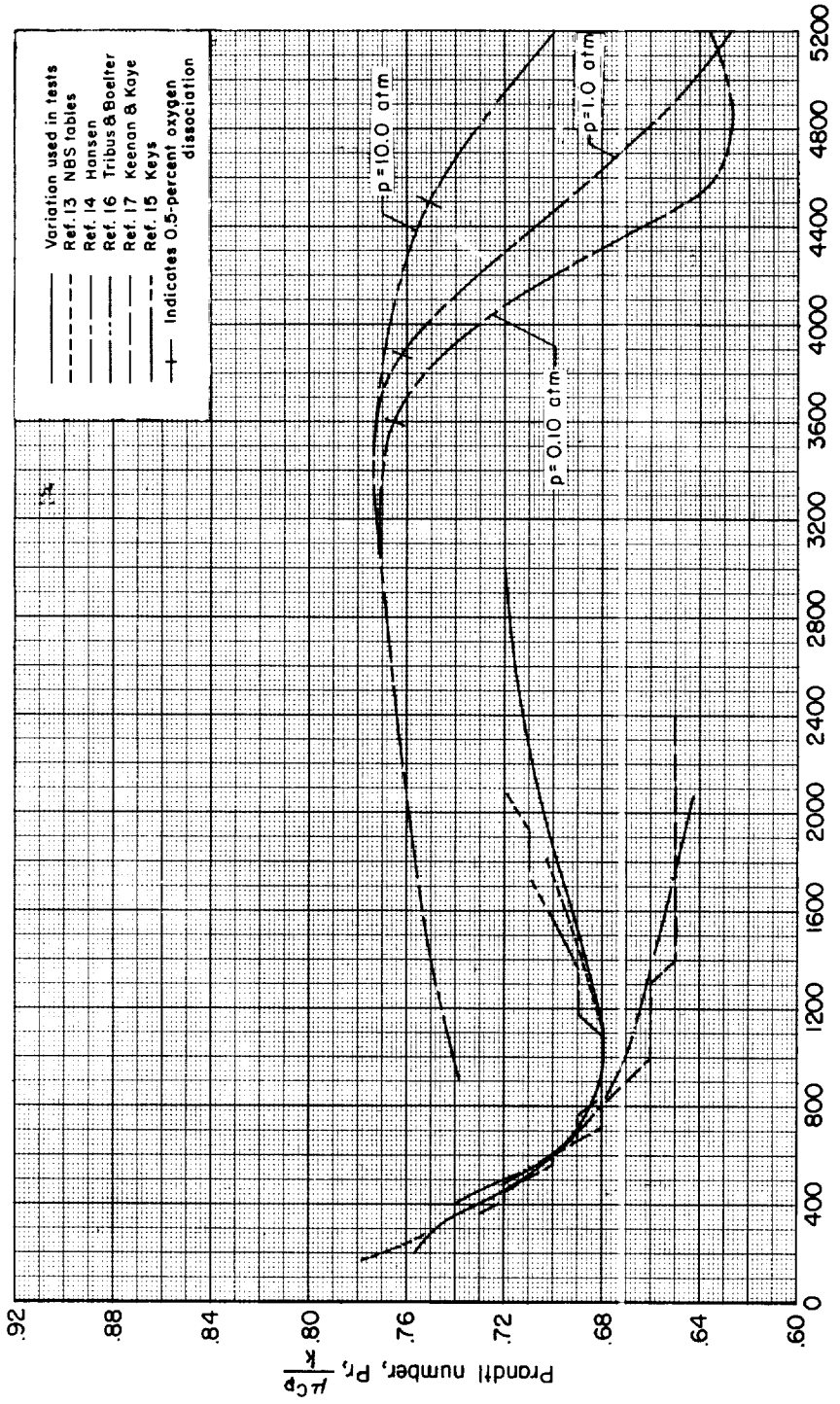

(e) Prandtl number, Pr.

Figure 5.- Concluded.

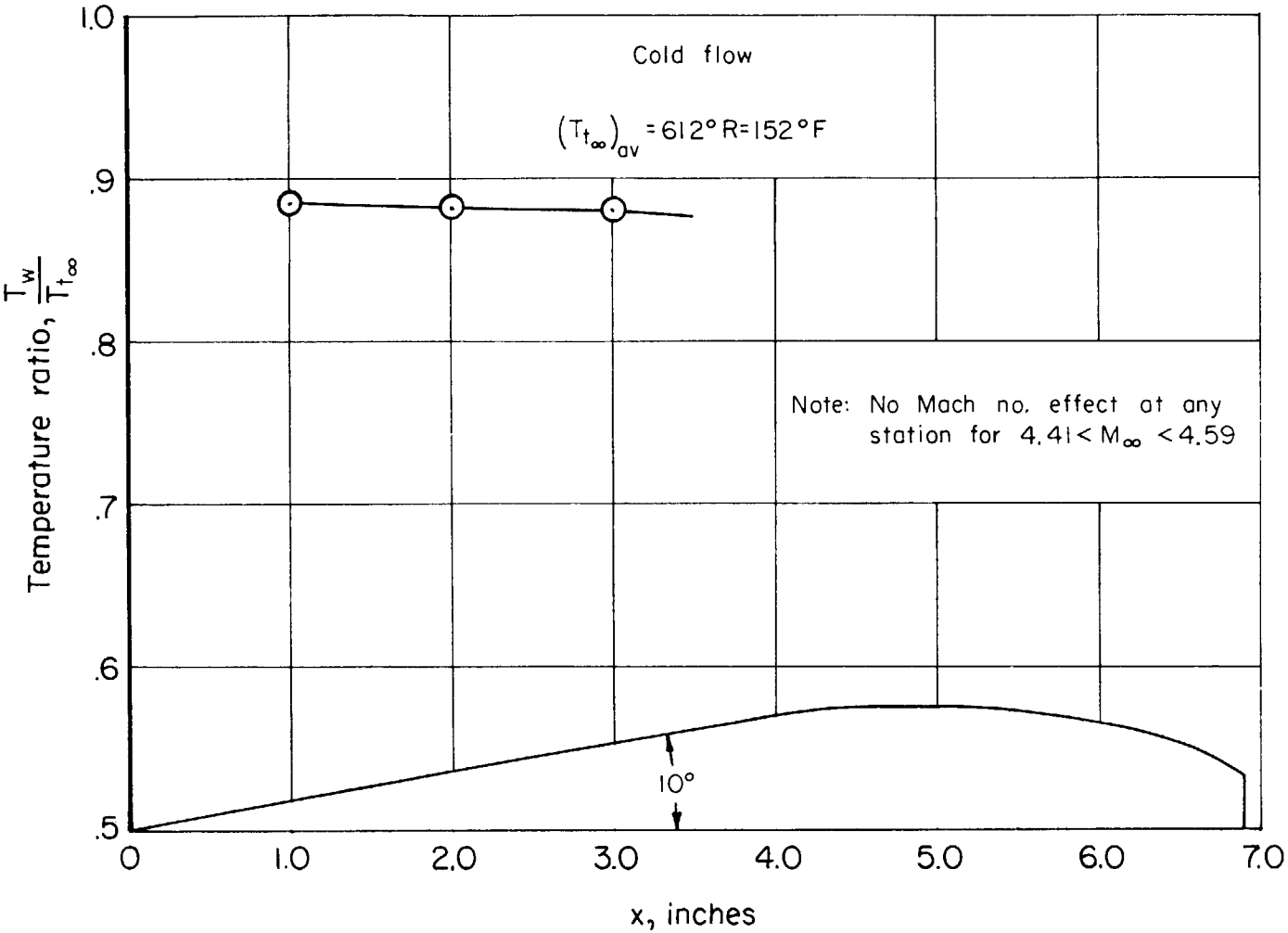

(a) Temperature ratio.

Figure 6.- The temperature ratio and recovery factor as a function of the distance along the model.

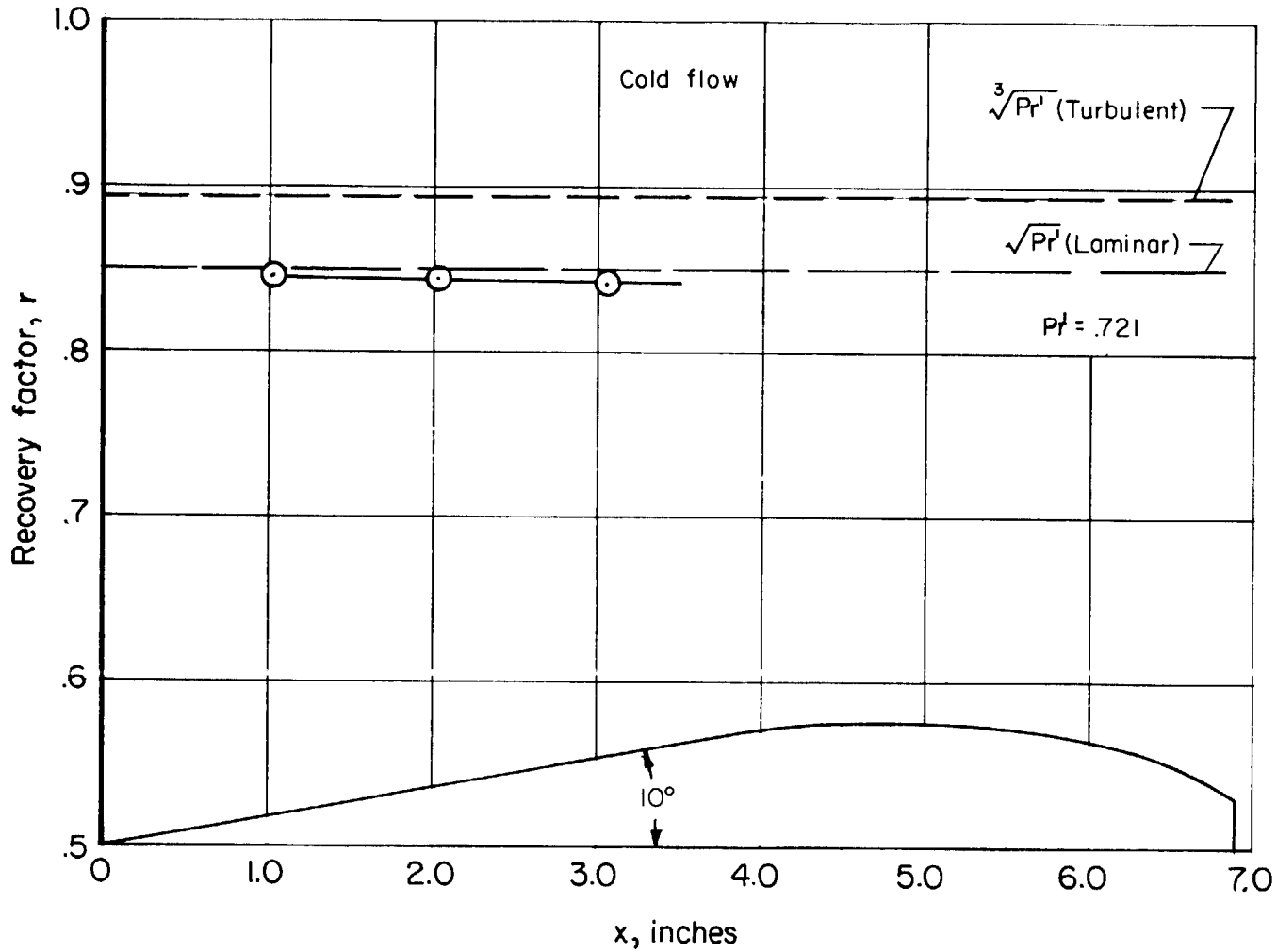

(b) Recovery factor.

Figure 6.- Concluded.

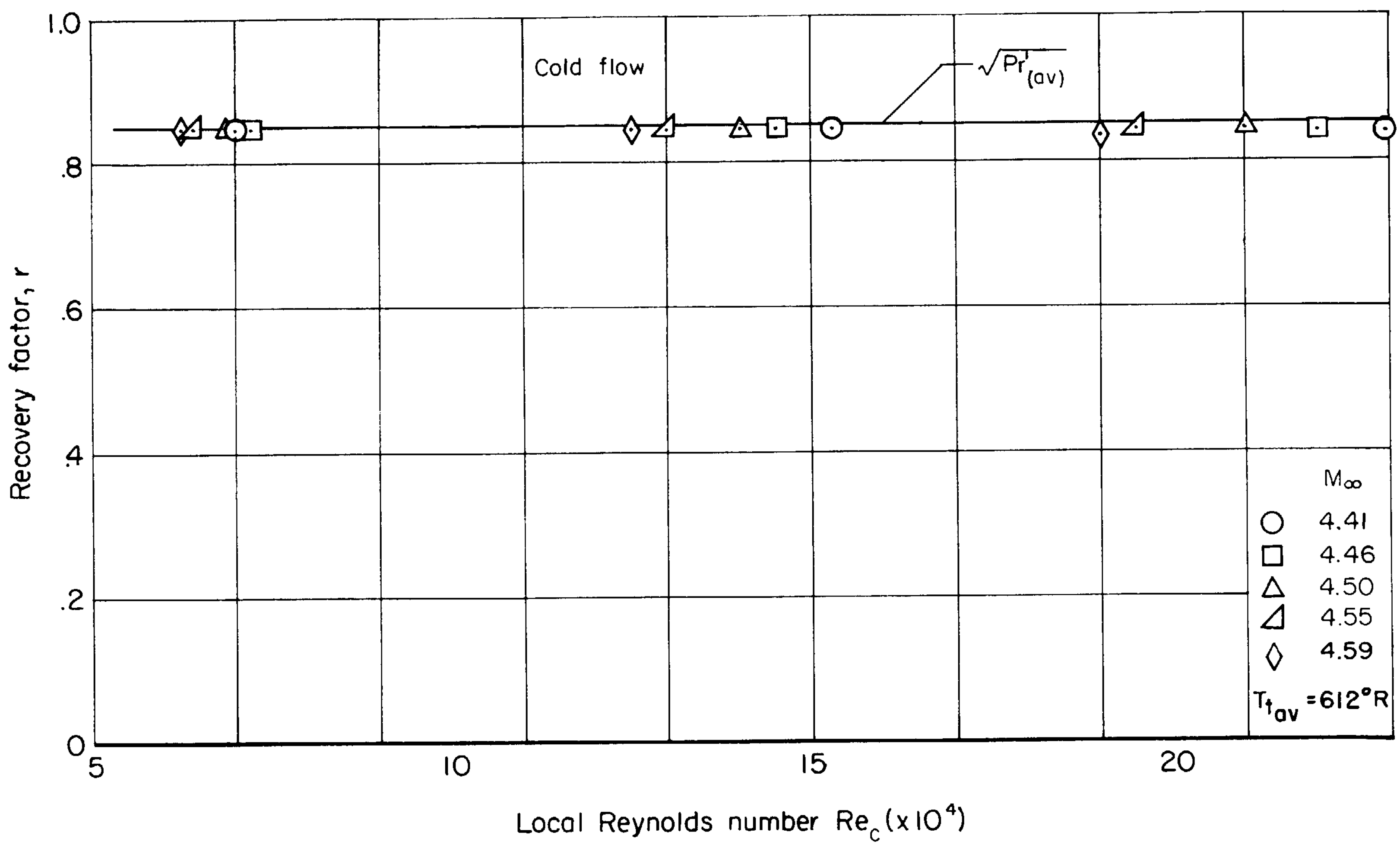

Figure 7.- Recovery factor as a function of local Reynolds number for the cold-flow model.

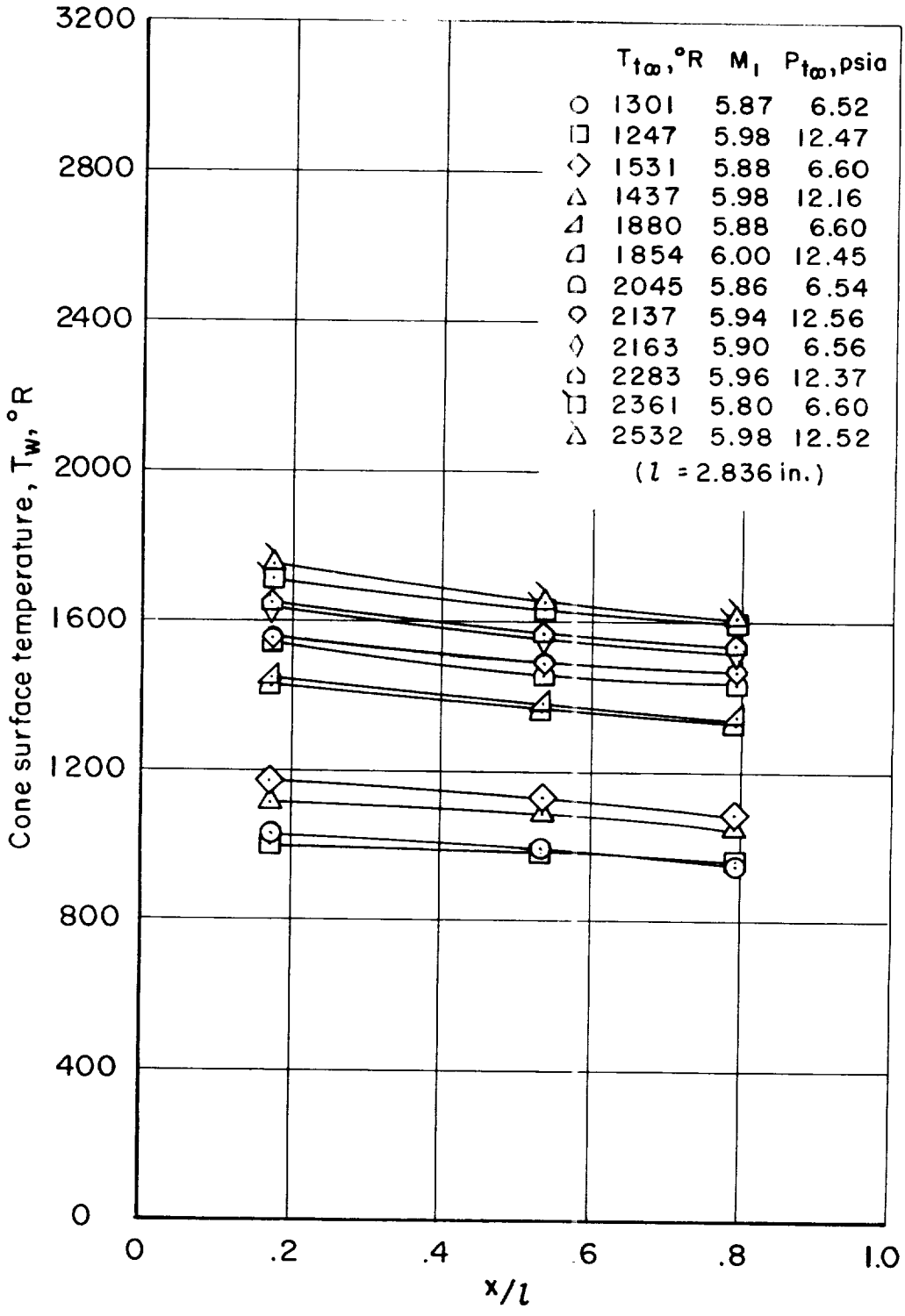

Figure 8.- Temperature distribution along hot-flow model.

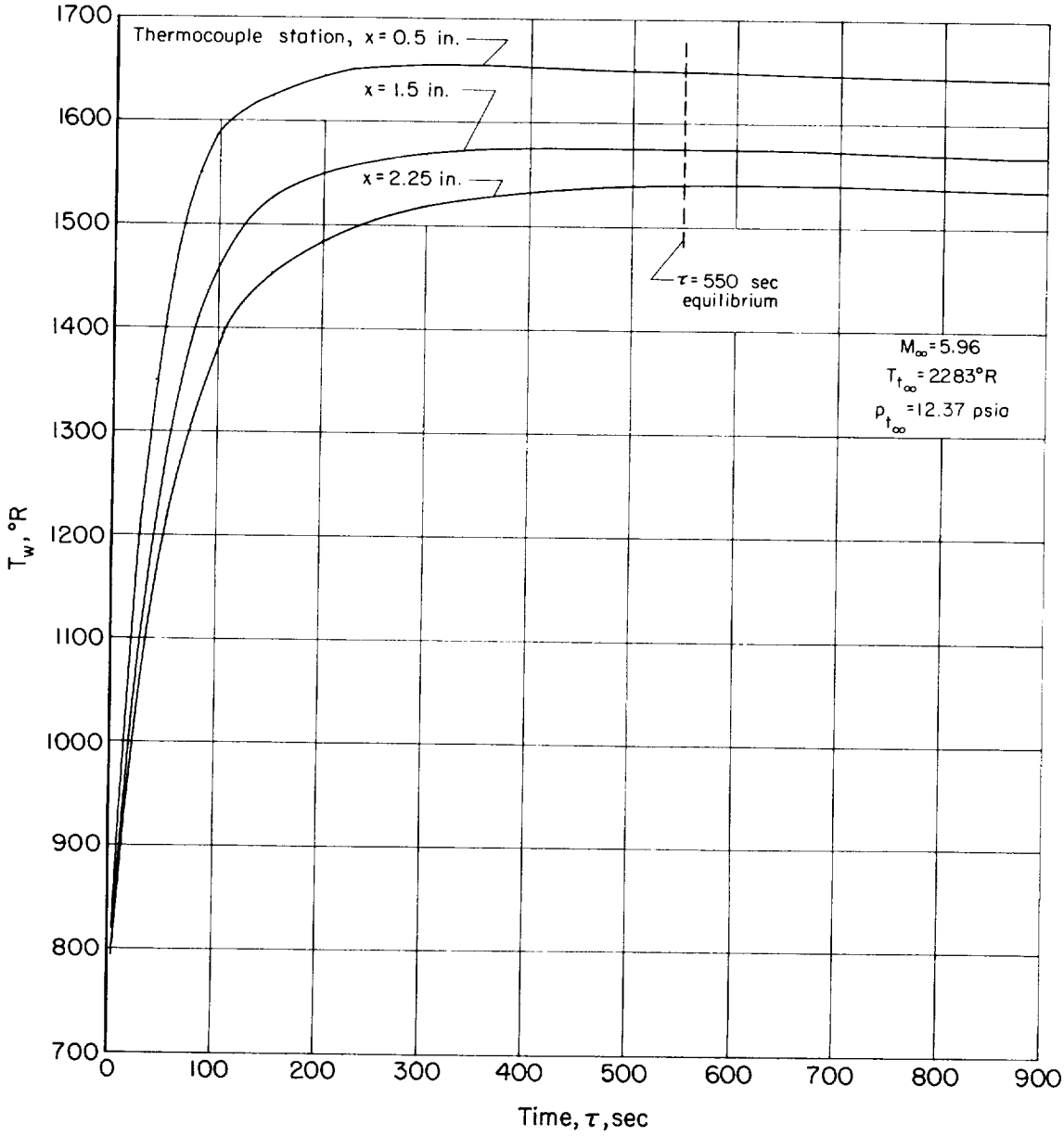

Figure 9.- Representative surface temperature-time history for hot-flow model.

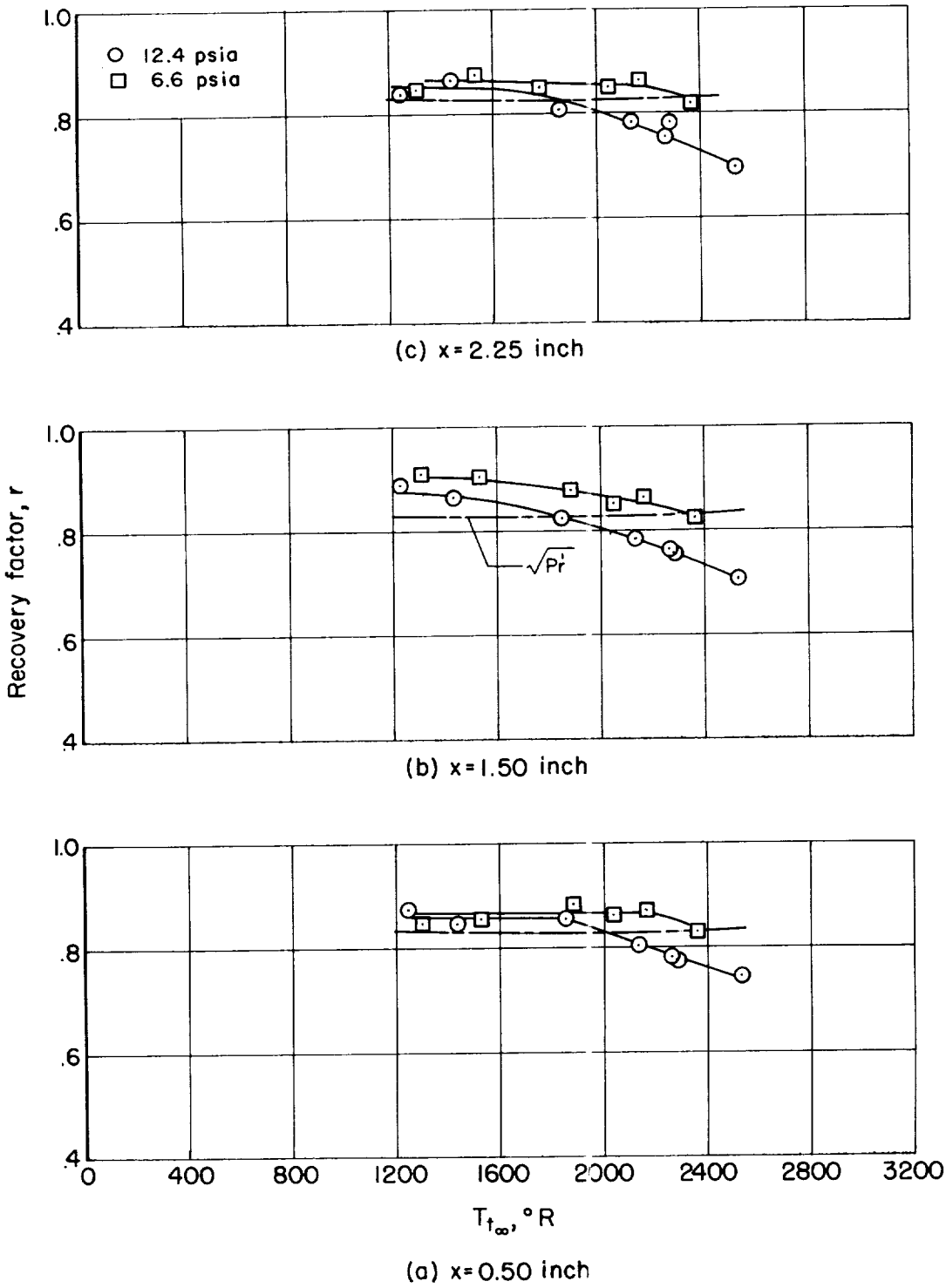

Figure 10.- Recovery factor as a function of free-stream total temperature.

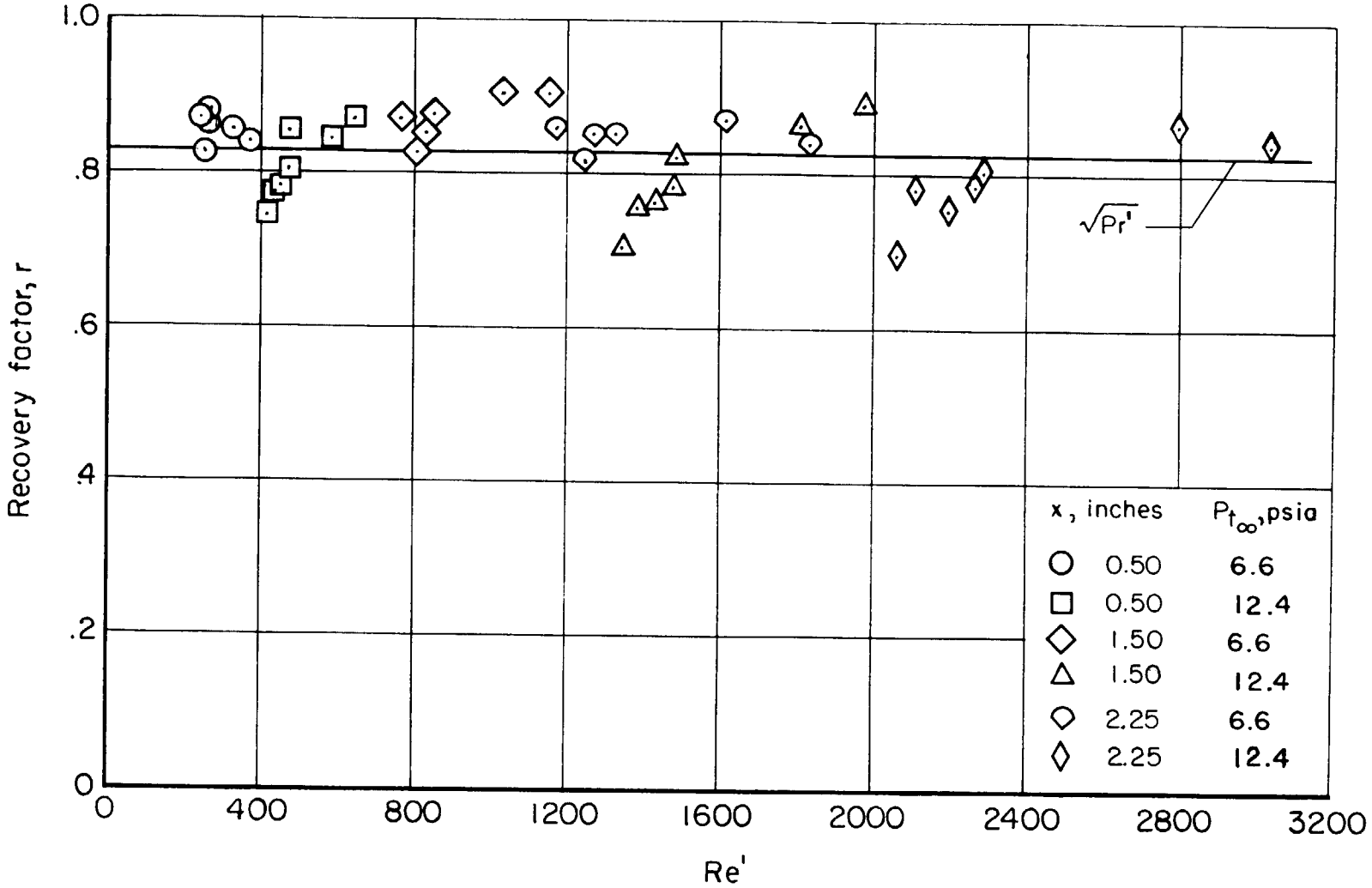

Figure 11.- Recovery factor as a function of the local Reynolds number based on T'; hot-flow model.

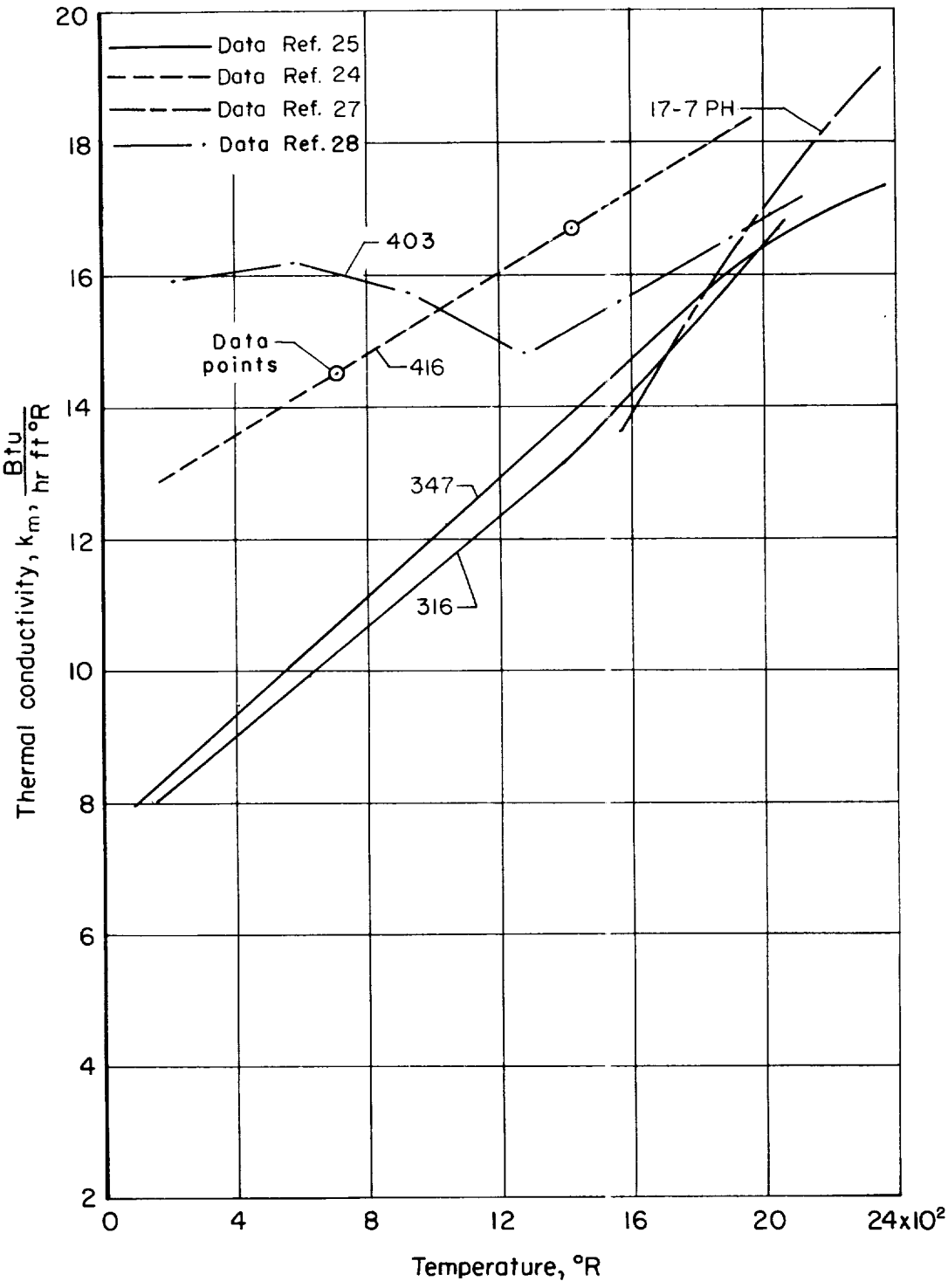

Figure 12.- Thermal conductivity of several types of stainless steel as a function of temperature.

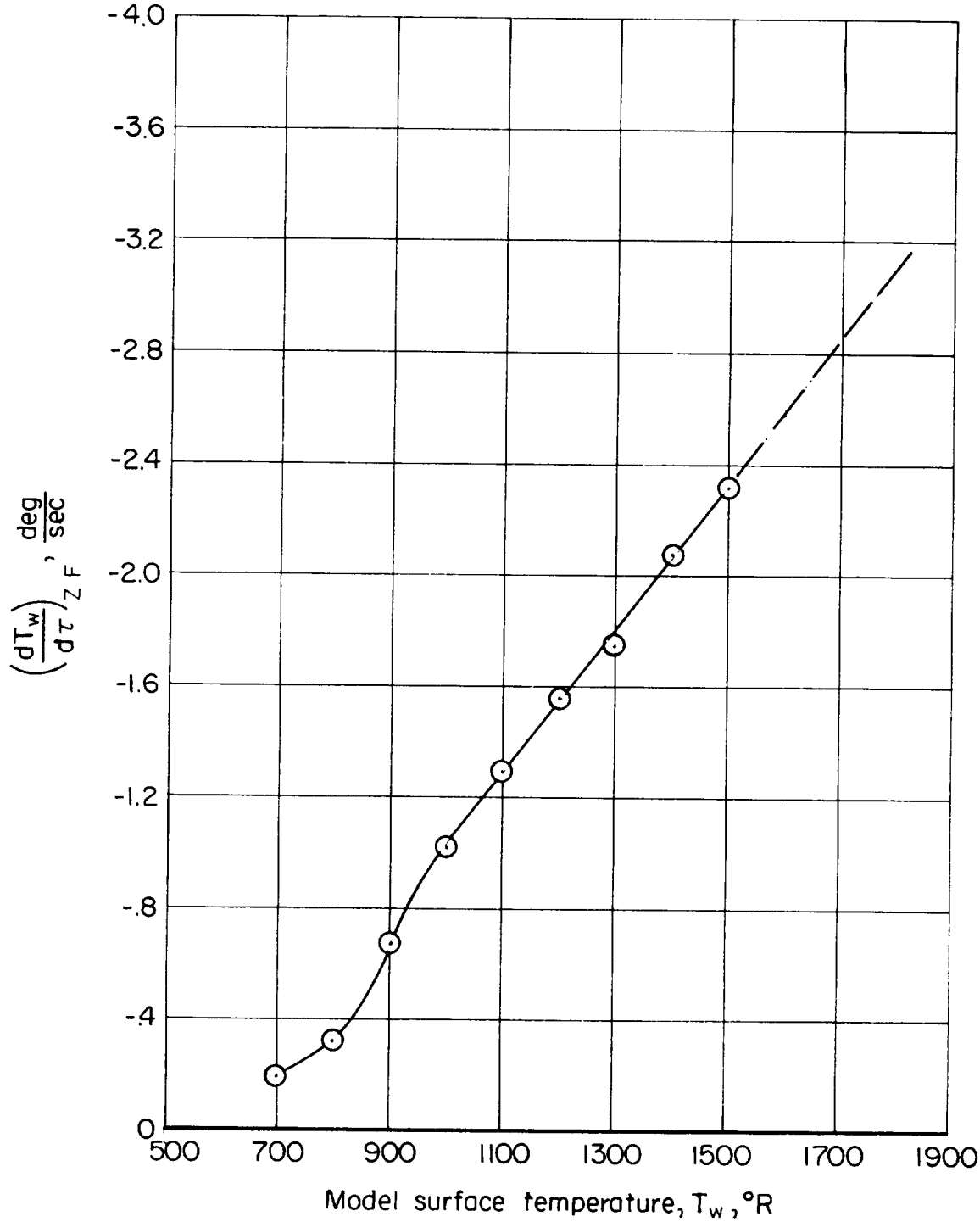

Figure 13.- Rate of change of surface temperature with time as a function of surface temperature for the radiation tare runs ($M_\infty = 0$, $p_{t_\infty} \cong 0$).

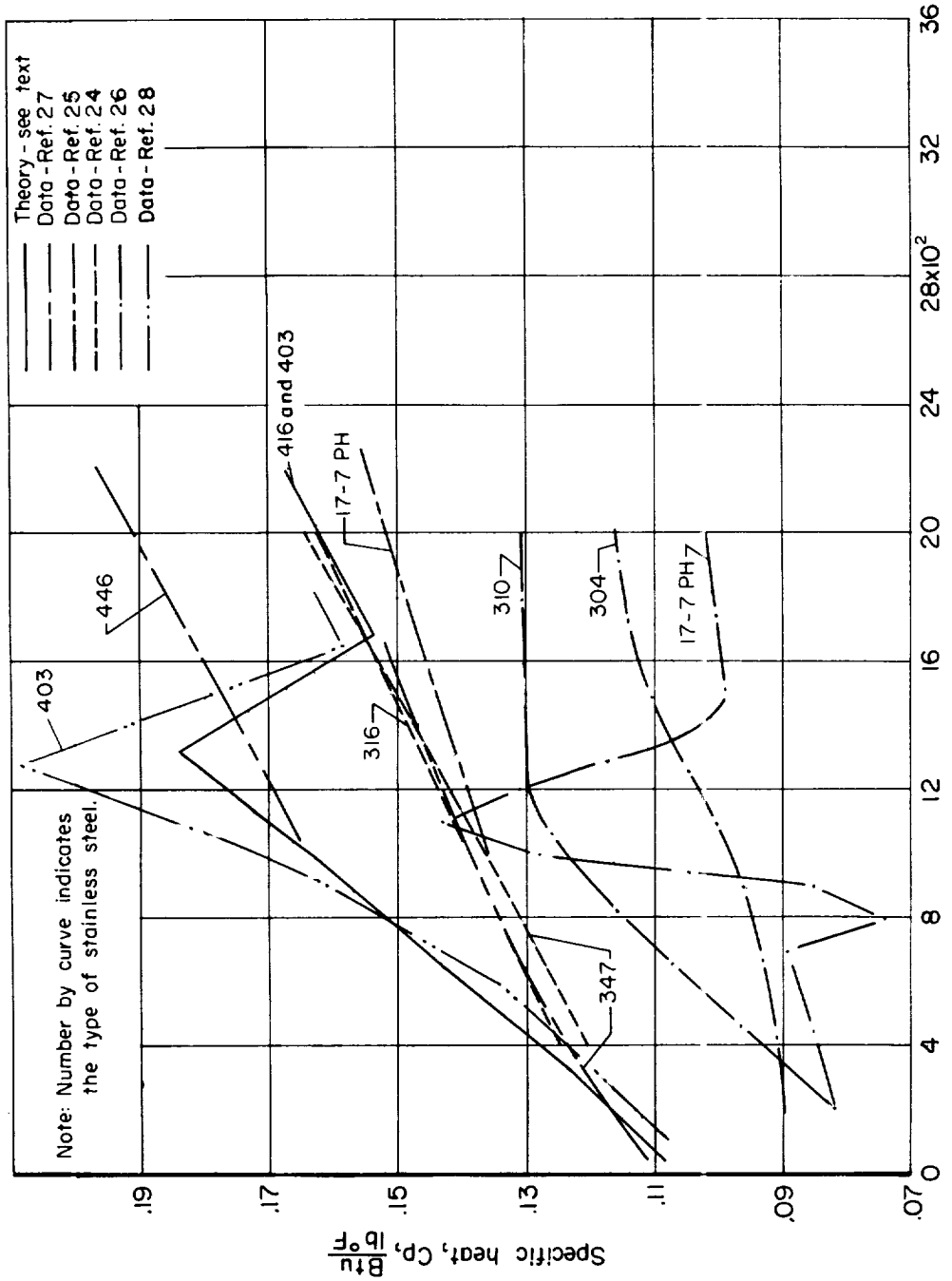

Figure 14.- Specific heat at constant pressure for several types of stainless steel as a function of temperature.

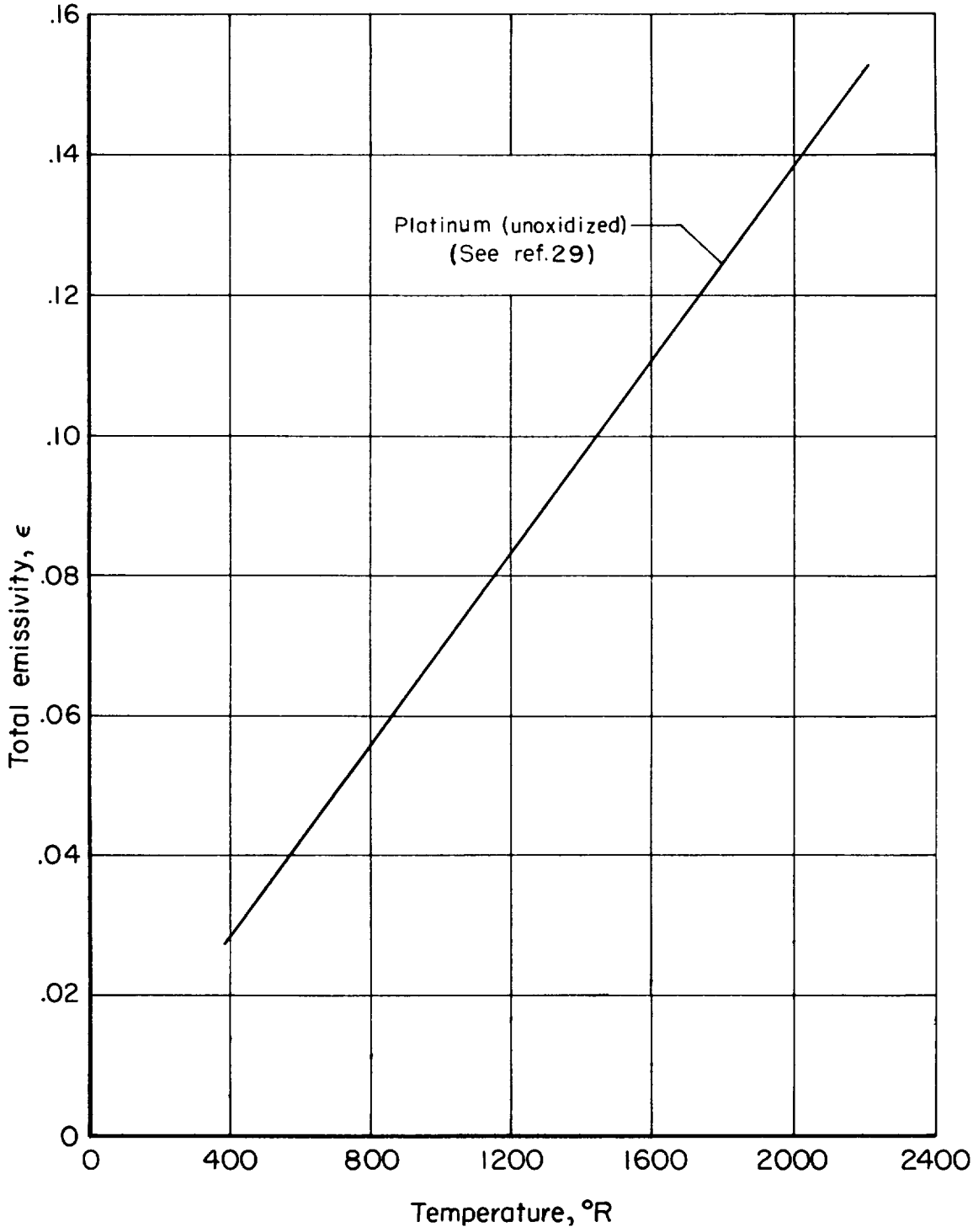

Figure 15.- Emissivity of unoxidized platinum as a function of temperature.

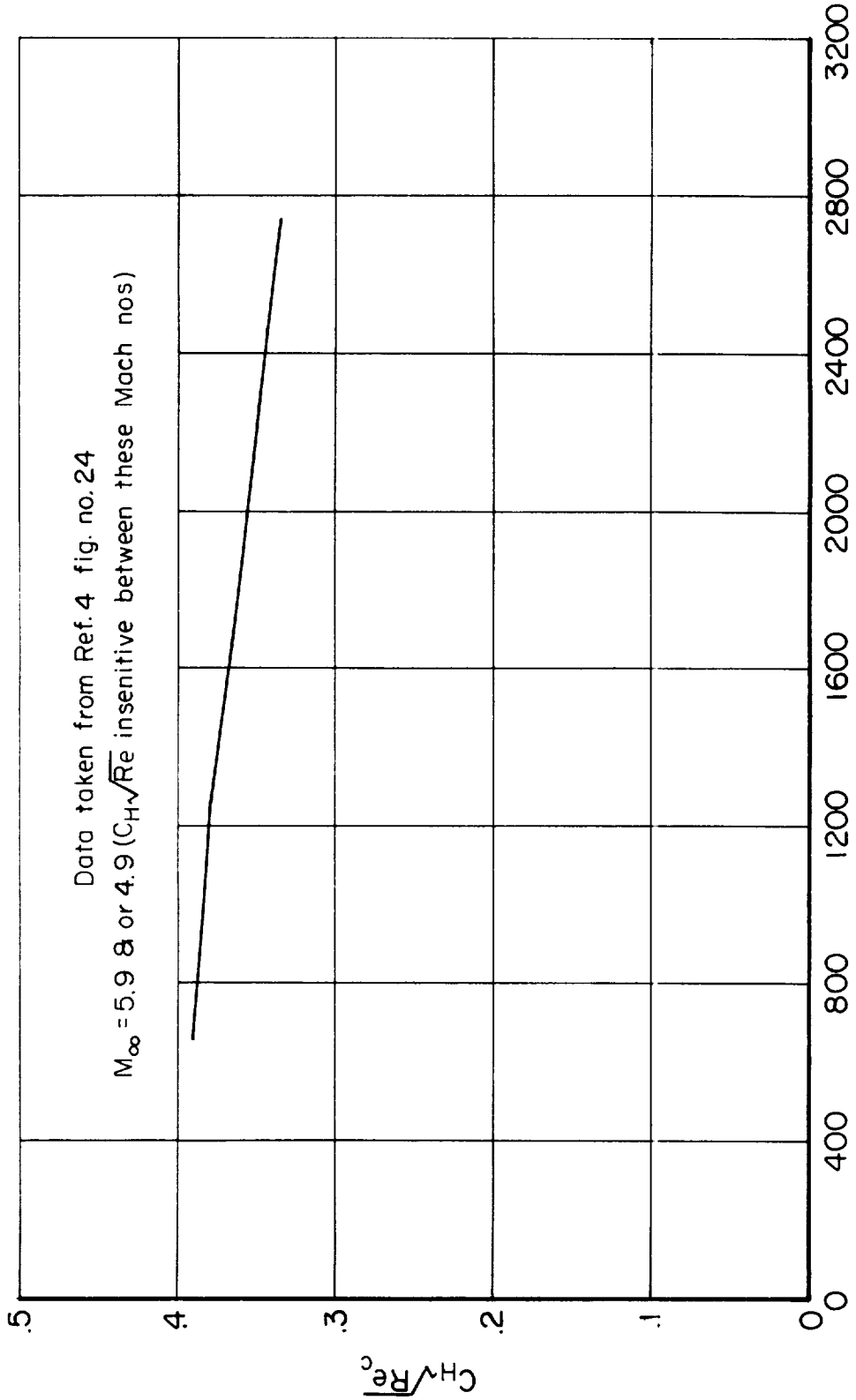

Figure 16.- Local heat-transfer parameter for a laminar boundary layer on an insulated flat plate as a function of stagnation temperature.